

Chapter 1

Introduction

In this thesis we investigate the large-scale configuration and dynamics of Saturn's magnetosphere, using *in situ* data and computer models. But first, we must consider the fundamental physics concepts that allow us to understand Saturn's magnetosphere, and the language we will use to describe it.

Saturn's magnetosphere comprises magnetic fields, electric fields and *plasma*. *Plasma* is considered the fourth state of matter after solid, liquid, and gas, and is formed of a gas that has been ionised, such that the atoms have been split up into negatively charged electrons and positively charged ions. Unlike neutral particles, charged particles are influenced by electric and magnetic fields, and this fundamentally determines how plasma behaves differently to other neutral states of matter. We therefore start this chapter with a discussion of how charged particles are affected by electromagnetic forces, and how we can understand these effects by considering the plasma as a bulk fluid. We then discuss the nature of the magnetised plasmas we encounter in space, moving outwards through the solar system from the Sun to Earth, Jupiter and finally Saturn. We provide details for the construction of a force-balance model of Saturn's *magnetodisc*, which is used throughout this thesis as a tool to explore the behaviour of Saturn's magnetosphere. We finish the chapter with a summary of the open questions in this area of research, some of which this thesis plans to address.

1.1 Physics of Magnetised Plasmas

1.1.1 Forces on an Individual Charged Particle

We begin with Maxwell's equations of electromagnetism. These are:

$$\nabla \times \mathbf{E} = -\frac{\partial \mathbf{B}}{\partial t} \quad (1.1)$$

$$\nabla \times \mathbf{B} = \mu_0 \mathbf{J} + \frac{1}{c^2} \frac{\partial \mathbf{E}}{\partial t} \quad (1.2)$$

$$\nabla \cdot \mathbf{E} = \frac{\rho_q}{\epsilon_0} \quad (1.3)$$

$$\nabla \cdot \mathbf{B} = 0. \quad (1.4)$$

These equations govern how electric (\mathbf{E}) and magnetic (\mathbf{B}) fields vary over time t and through space. \mathbf{J} is the current density, ρ_q is the charge density, $c^2 = 1/\mu_0\epsilon_0$ is the square of the speed of light, and μ_0 and ϵ_0 are the constants known as the permeability and permittivity of free space. Together with the Lorentz force law, we can use these equations to understand how a charged particles interact with electric and magnetic fields. The Lorentz force is given by

$$\mathbf{F}_L = q(\mathbf{E} + \mathbf{v} \times \mathbf{B}), \quad (1.5)$$

where q is the charge of the particle and \mathbf{v} its velocity. In the absence of an electric field, and with a uniform magnetic field, it can be shown that this Lorentz force causes the charged particle to gyrate around the magnetic field direction, with angular frequency

$$\Omega_c = \frac{|q|B}{m} \quad (1.6)$$

known as the cyclotron frequency, where m is the mass of the particle and B is the magnitude of the magnetic field. From equation 1.5 with $\mathbf{E} = 0$, positively charged particles gyrate in a left-handed sense around the magnetic field, and negatively charged particles gyrate in a right-handed sense. The radius of this orbit is given by the gyroradius, or Larmor radius,

$$r_L = \frac{v_\perp}{\Omega_c} = \frac{mv_\perp}{|q|B} \quad (1.7)$$

where \perp and later \parallel subscripts refer to components perpendicular and parallel to the magnetic field. r_L is generally larger for ions (which are more massive than electrons), and for particles with higher energy (and so higher v_\perp). Note that the Lorentz force acts perpendicular to the magnetic field by definition, and so the motion of charged particles *parallel* to the magnetic field is not affected by \mathbf{B} ; charged particles are thus free to move up and down along magnetic field lines, in the absence of other forces.

In a spatially non-uniform magnetic field, a particle will not only gyrate around a magnetic field line, but the guiding centre of its gyroscopic motion will also drift, depending on the variation of the magnetic field. The velocity of this guiding-centre motion is given by the gradient drift velocity

$$\mathbf{v}_g = \frac{mv_\perp \mathbf{B} \times \nabla B}{2qB^3} \quad (1.8)$$

and is therefore in a direction perpendicular to both the magnetic field direction and the gradient of the magnetic field magnitude. In an approximately dipolar magnetic field, e.g. at Saturn, the magnetic field strength decreases with radial distance, and so ∇B is oriented radially inwards, while the magnetic field \mathbf{B} is oriented downwards near the equator (or upwards at other magnetised planets, such as Earth and Mercury). At Saturn, this has the net effect of causing positively charged ions to drift eastwards, and negatively charged electrons to drift westwards, which sets up a net flow of charge (i.e. current) eastwards, in the direction of planetary rotation.

In a dipolar magnetic field, the magnetic field lines are also curved, and so a charged particle gyrating and also moving freely along a magnetic field line will feel a centrifugal force. This force also induces a drift in the guiding centre of the charged particle's orbit, given by the curvature drift velocity

$$\mathbf{v}_c = \frac{mv_\parallel^2 \mathbf{r}_c \times \mathbf{B}}{qB^2 r_c^2} \quad (1.9)$$

where \mathbf{r}_c is the radius of curvature vector for the magnetic field line, defined as pointing radially outwards from the centre of curvature to the particle. (As an example, for a dipole magnetic field $r_c = r/3$ at the magnetic equator, where r

is the radial distance from the origin.) This therefore has the same effect as the gradient drift force, with ions drifting eastwards and electrons drifting westwards, resulting in a net current in the direction of planetary rotation.

For a general external force \mathbf{F} the guiding-centre drift associated with that force is given by

$$\mathbf{v}_F = \frac{\mathbf{F} \times \mathbf{B}}{qB^2}. \quad (1.10)$$

For the case $\mathbf{F} = q\mathbf{E}$, the force exerted by an electric field \mathbf{E} , then the q term on the denominator of equation (1.10) cancels, and \mathbf{v}_F is independent of q such that both electrons and ions drift in the same direction.

Finally, it is important to consider the phenomenon of magnetic mirroring of charged particles, as this dynamical effect is common in the approximately dipolar magnetic fields of magnetised planets. The magnetic moment μ_m of a charged particle gyrating in a circular orbit around a magnetic field with gyroradius r_L , can be written as

$$\mu_m = \frac{mv_\perp^2}{2B} \quad (1.11)$$

from the definition $\mu = IA$, with $I = q\Omega_c/2\pi$ and $A = \pi r_L^2$. For a slowly varying magnetic field, this quantity is conserved and is known as the *first adiabatic invariant*. A consequence of this is that as a particle gyrates along a magnetic field line towards a region where the magnetic field strength increases (e.g. polar regions of a dipole magnetic field), the particle's perpendicular velocity v_\perp must also increase. Without an external electric field to do work on the particle, the total energy of the particle $\frac{1}{2}m(v_\perp^2 + v_\parallel^2)$ must remain constant, and so an increase in v_\perp coincides with a decrease in v_\parallel , until v_\parallel reaches zero and the particle is 'reflected' back along the magnetic field line in the opposite direction. That is, the motion of the guiding centre of the particle motion reverses direction. This phenomenon causes charged particles to 'bounce' up and down along dipolar magnetic field lines, reflecting near the poles where the magnetic field strength acquires a value large enough to reverse the guiding centre motion.

Therefore, charged particles in a planetary dipole magnetic field simultaneously gyrate around the magnetic field lines, bounce up and down along them, and drift azimuthally around the planet in a direction depending on their charge.

1.1.2 Forces on a Collective Plasma

Considering the motion of individual charged particles can only get us so far when trying to understand the global dynamics of large-scale plasma structures, such as planetary magnetospheres. It can be helpful to describe the plasma as a single fluid, with a bulk plasma flow velocity \mathbf{u} . This approach is known as single fluid magnetohydrodynamics (MHD), and the *momentum equation* for the plasma fluid is given by

$$\rho \frac{d\mathbf{u}}{dt} = \rho_q \mathbf{E} + \mathbf{J} \times \mathbf{B} - \nabla P + \rho \mathbf{g} \quad (1.12)$$

where ρ is the mass density of the plasma, P is the plasma pressure (assumed to be isotropic), and \mathbf{g} is the acceleration due to gravity. The first terms on the right hand side correspond to the Lorentz force terms given in equation 1.5 for the bulk plasma. However if we assume quasi-neutrality, such that the density of ions and the density of electrons in the plasma are approximately equal, then ρ_q is negligible and we can ignore the effect of the electric field \mathbf{E} . This is appropriate when considering plasmas over large temporal or spatial scales, as the individual charged particles quickly adjust to remove any charge imbalance caused by local density variations. Similarly in most space plasmas we can neglect the gravitational term as being insignificant compared to other terms.

This leaves the plasma pressure gradient force and the $\mathbf{J} \times \mathbf{B}$ force as the dominant forces on the magnetised plasma. To understand the effect of the $\mathbf{J} \times \mathbf{B}$ force in particular on the plasma, it is helpful to consider the case where plasma flows are significantly slower than the speed of light, which is appropriate for space plasmas considered in this thesis. In this case, we can neglect the second ‘displacement current’ term in the Maxwell’s equation known as the Ampère-Maxwell relation (equation 1.2), and so this simplifies to

$$\nabla \times \mathbf{B} = \mu_0 \mathbf{J} \quad (1.13)$$

known as Ampère’s Law. This allows the $\mathbf{J} \times \mathbf{B}$ force to be rewritten as

$$\mathbf{J} \times \mathbf{B} = -\nabla \left(\frac{B^2}{2\mu_0} \right) + \frac{1}{\mu_0} (\mathbf{B} \cdot \nabla) \mathbf{B}. \quad (1.14)$$

The first term on the right hand side corresponds to a magnetic pressure gradient

force, with magnetic pressure $P_B = B^2/2\mu_0$. The second term on the right hand side corresponds to the magnetic tension force. The component of this force perpendicular to the magnetic field direction, known as the curvature force, acts to ‘straighten’ bent field lines, akin to the restoring force on a bent elastic band, and scales with the magnetic field strength and radius of curvature as B^2/r_c . The component of this force parallel to the magnetic field lines cancels out exactly with the parallel component of the magnetic pressure gradient force, as the total $\mathbf{J} \times \mathbf{B}$ force must act perpendicular to the magnetic field by definition.

We will return to these concepts of magnetic pressure and tension forces, and discuss force balance in the plasma in these terms throughout this thesis.

1.1.3 The Frozen-in Field Theorem

If we make a few more simplifying assumptions about the nature of our plasma, we have conditions for *ideal MHD*. In particular we assume the plasma conditions do not vary on length scales and time scales smaller than the particle gyroradius nor the associated gyroperiod. We also assume the conductivity of the plasma is sufficiently high that we can neglect Joule heating, resistivity and collisions between particles, which is appropriate for the collisionless space plasmas that we consider in this thesis. This leads us to the idealised Ohm’s Law,

$$\mathbf{E} + \mathbf{u} \times \mathbf{B} = 0 \quad (1.15)$$

An important mathematical consequence of this is the *frozen-in field theorem*. This powerful theorem states, under the conditions as described above, that the plasma and the magnetic field are ‘frozen in’ to each other and move together. From equation 1.15 it can be shown that if a magnetic field threads through two plasma fluid elements, the field will continue to connect them even as the elements move and change shape and size. This also means that two different plasma populations embedded with different magnetic fields cannot mix.

This theorem is instructive in intuitively understanding the behaviour of many space plasmas, including planetary magnetospheres. To determine whether the plasma approximately follows the magnetic field, or the magnetic field approximately follows the plasma, it is useful to consider the quantity plasma β , defined

as

$$\beta = \frac{P}{B^2/2\mu_0} \quad (1.16)$$

the ratio of the plasma to magnetic pressure. In high β ($>> 1$) regimes, the plasma dominates, and the magnetic field that threads the plasma is convected along with the plasma flow. In low $\beta < 1$ regimes, the opposite is the case, and the plasma is locked into the moving magnetic field. Both regimes are found in space plasmas (discussed in the rest of this chapter), and we will encounter both regimes in our study of Saturn's magnetosphere in this thesis. In particular we will often refer to 'flux tubes' of plasma in Saturn's magnetosphere, which are volumes of plasma mapped out by the planetary dipole magnetic field lines, and which obey this frozen-in condition.

When the magnetic field varies on length scales comparable to the gyroradius of the individual plasma particles, ideal MHD breaks down and the frozen-in field theorem no longer holds. In this case, we observe a phenomenon known as *reconnection*, where magnetic field lines that were previously separated by different plasma populations are forced close enough together that they reconnect. This can cause an explosive release of plasma along the newly reconnected magnetic field lines, and a reconfiguration of the magnetic field. This is a fundamental process in planetary magnetospheres, as discussed in more detail in Section 1.3.3.

1.1.4 Plasma Waves

Many different types of waves can be set up in magnetospheric plasma populations. If we assume these waves are small in amplitude and thus only cause first-order perturbations to the background plasma properties (represented by the subscript 0 in the following equations), then we can use MHD to characterise their propagation speeds. The speed of sound in the plasma is defined as

$$c_s = \sqrt{\frac{\gamma P_0}{\rho_0}}, \quad (1.17)$$

as for a classical gas, where γ is the ratio of specific heats. If we assume the plasma is incompressible, and *cold* such that $P_0 = c_s = 0$, the MHD relations we have

discussed can be used to derive the dispersion relation for the plasma:

$$\omega^2 = k^2 v_A^2 \cos^2 \theta \quad (1.18)$$

where ω is the wave angular frequency, k is the wave number and θ is the angle between the wave propagation direction and the background magnetic field direction. v_A is a characteristic speed known as the *Alfvén speed*,

$$v_A = \frac{B_0}{\sqrt{\mu_0 \rho_0}}. \quad (1.19)$$

Physically, oscillations in the magnetic field travel along the background magnetic field direction at this speed, analogous to waves propagating on a massive string. As shown by equation 1.18, the phase velocity depends on θ , and is maximum (equal to v_A) for propagation parallel to the magnetic field, and minimum (0) for propagation perpendicular to the field.

If instead we consider a *warm* plasma and include the effect of plasma pressure, this dispersion relation becomes

$$\frac{\omega^2}{k^2} = \frac{1}{2} \left(c_s^2 + v_A^2 \pm \sqrt{(c_s^2 + v_A^2)^2 - 4c_s^2 v_A^2 \cos^2 \theta} \right) \quad (1.20)$$

where the \pm introduces two different wave modes, known as the *fast* and *slow* modes. While this dispersion relation may seem complicated, interesting results fall out when the parallel ($\cos \theta = 1$) and perpendicular ($\cos \theta = 0$) propagation cases are considered separately. In the limit of parallel propagation, the two wave modes propagate at the Alfvén speed v_A and the sound speed c_s respectively. For low β plasmas, $c_s < v_A$ and so v_A is considered the *fast* mode, while the opposite is the case for high β plasmas. In the limit of perpendicular propagation, the *slow* mode vanishes to zero, and the *fast* mode propagates at the characteristic speed known as the *magnetosonic speed* c_{ms} ,

$$c_{ms} = \sqrt{v_A^2 + c_s^2}. \quad (1.21)$$

Other types of waves can also be set up in magnetised plasmas, depending on the conditions. However for the magnetospheric plasma environments we discuss in this thesis, an understanding of the Alfvén, sound and magnetosonic speeds is

sufficient.

1.2 The Solar Wind

The corona is the uppermost atmospheric layer of the Sun, and is composed mainly of ionised hydrogen (i.e. protons and electrons), with approximately 4% ionised helium (?). This layer is heated from below by fusion processes in the deep interior, and other processes not yet fully understood, to extremely high temperatures of $\sim 10^6 \text{ K}$ (?). Above, the corona is surrounded by relatively empty space, and thus experiences a large thermal pressure gradient force directed radially outwards. This means that a significant fraction of the coronal plasma is energetic enough to escape the Sun's strong gravitational field, and thus streams radially outwards from the Sun through space at high speeds. This plasma flow is known as the solar wind.

The properties of the solar wind vary on many timescales, however it is still useful to consider the typical properties. The typical solar wind speed is around 450 km s^{-1} throughout the solar system, well above the local speed of sound. The particle number density falls approximately as r^{-2} (the inverse square of radial distance from the Sun) in line with conservation of particle flux through an expanding spherical surface, with density from around 7 cm^{-3} at the orbit of Earth (1 AU) to 0.07 cm^{-3} at the orbit of Saturn (9.6 AU) (where $1 \text{ AU} = 1.496 \times 10^8 \text{ km}$) (?). Near the solar surface, the strong and complex magnetic field of the Sun dominates the plasma, in line with the frozen-in field theorem for low β plasmas, and so generates phenomena such as coronal loops. However, further away from the Sun, beyond a few tens of solar radii, the magnetic field strength decreases with radial distance such that β increases and the remnant magnetic field becomes frozen-in to the moving solar wind plasma (?). The magnetic field is therefore carried outwards into space by the flowing plasma, where it is known as the interplanetary magnetic field (IMF). The radial outflow of the solar wind, combined with the ~ 25 day rotation period of the Sun, produce a spiral-like distribution of magnetised plasma in the Sun's equatorial plane which extends throughout the solar system, known as the *Parker Spiral* (?). This structure influences the typical orientation of the interplanetary magnetic field observed at each planet, from approximately radial at the orbit of Mercury, to approximately perpendicular to the radial flow at the orbit of Saturn. Figure 1.1 shows a diagram of this phenomenon. The orientation of the IMF has consequences

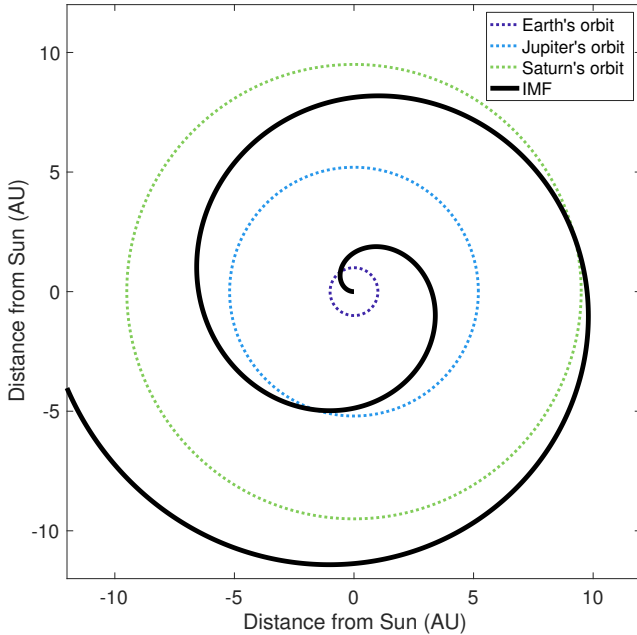


Figure 1.1: Diagram showing how the Parker Spiral affects the orientation of the IMF (interplanetary magnetic field) in the equatorial plane throughout the solar system. The orbits of different planets are shown by the coloured dotted lines.

for the interaction between the solar wind and the planet, as discussed in future sections.

On top of this rotating structure, the properties of the solar wind vary on timescales ranging from minutes to years. At the shorter end of the time spectrum, coronal mass ejections (CMEs) are dynamic outflows of dense, coronal material that occur due to dramatic reconfiguration of the coronal magnetic field. These typically form over days and may reach speeds as high as several thousand km s^{-1} as they accelerate through the inner solar system. Their movements are associated with regions of enhanced density and magnetic field strength compared to the ambient solar wind (?). At the opposite end of the spectrum, it is well known that the Sun exhibits periodic behaviour with an approximately 11 year cycle, known as the solar cycle. This cycle of alternatively high and low solar activity can be tracked well by the number of sunspots that appear on the solar surface, and is correlated with solar wind properties such as solar irradiance, magnetic field strength, and flare and CME incidences (?). There is therefore a great deal of variability in the magnetic and plasma environment of the solar system, over time and through space.

1.3 Planetary Magnetospheres

1.3.1 Structure of a Magnetosphere

A magnetosphere is a ‘bubble’ of magnetised plasma that surrounds a planet with a significant internal magnetic field, and forms due to the interaction between this magnetic field and the solar wind. Mercury, Earth, and the outer giant planets all have approximately dipolar internal magnetic fields, generated by convective flow of electrically conducting fluid in the planets’ deep interiors; thus they all have stable magnetospheres (?).

The magnetopause is the surface that separates the internal planetary plasma of the magnetosphere from the external shocked solar wind plasma of the magnetosheath. The magnetosheath is the region between the magnetosphere proper and the bow shock, where the solar wind plasma is decelerated to subsonic speeds. In a steady state system, the shape and size of the magnetopause is determined by pressure balance across the boundary, between the internal magnetic and plasma pressures, and the external solar wind pressure. The magnetopause morphology turn influences the configuration of the magnetosphere internally. Therefore, the structure of the magnetosphere varies significantly between different planets, where both the internal and external conditions are different. However, many features are broadly common to all planetary magnetospheres in some form, and Figure 1.2 shows a diagram specifically of Earth’s magnetosphere, with these main features labelled. Note that at Jupiter and Saturn, the internal planetary magnetic field is oppositely oriented such that the magnetic fields and current systems are all in the opposite direction.

It can be seen that the magnetosphere is approximately dipolar in configuration on the dayside (i.e. the side facing the Sun), with a more extended ‘tail’ on the nightside (i.e. the anti-sunward side), where the magnetic field lines stretch radially outwards and become approximately parallel to the solar wind direction. This tail can extend to tens or hundreds of planetary radii downstream of the planet; Jupiter’s magnetotail has even been observed to extend as far as the orbit of Saturn, corresponding to several thousand Jovian radii downstream (?). Figure 1.2 shows an azimuthal ring current system which orbits the planet, centred around the equatorial plane; the direction is determined by the direction of the curvature and

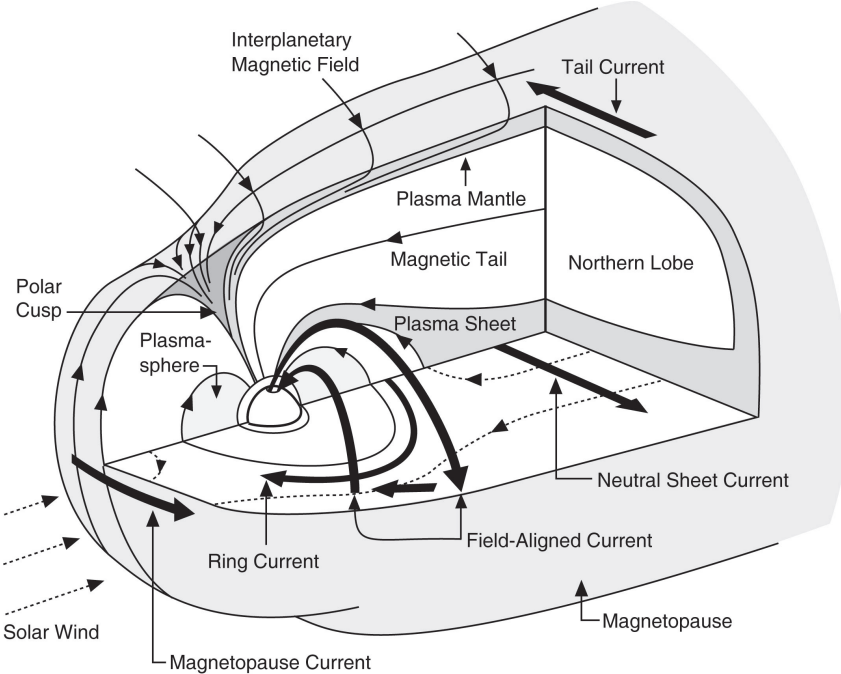


Figure 1.2: Diagram of the main features of Earth’s magnetosphere from ?, reproduced with permission.

gradient drift velocities for positively and negatively charged particles in Earth’s magnetic field, as described in Section 1.1.1 for the oppositely-oriented Saturn case. On the nightside this ring current extends into a current sheet, which separates the oppositely directed magnetic field lines in the northern and southern ‘lobes’ of the nightside magnetosphere. Currents also flow on the magnetopause and magnetotail surfaces as shown, separating the magnetic fields of the magnetosphere and the solar wind IMF. At the polar cusps, the magnetosphere is said to be ‘open’ to the solar wind, as in these regions the confined internal planetary dipole magnetic field structure changes in strength and direction over relatively small spatial scales and so allows solar wind particles to access the magnetosphere. This is in contrast to the more ‘closed’ regions of the magnetosphere, where it is difficult for solar wind particles to penetrate.

1.3.2 Comparative Magnetospheres

A comparison of the magnetospheres of different planetary systems is shown in Figure 1.3. The most striking difference is in the overall size of the magnetospheres, and this is mainly due to the twin influences of the external solar wind conditions at each planet, and internal magnetic pressure associated with the planetary magnetic

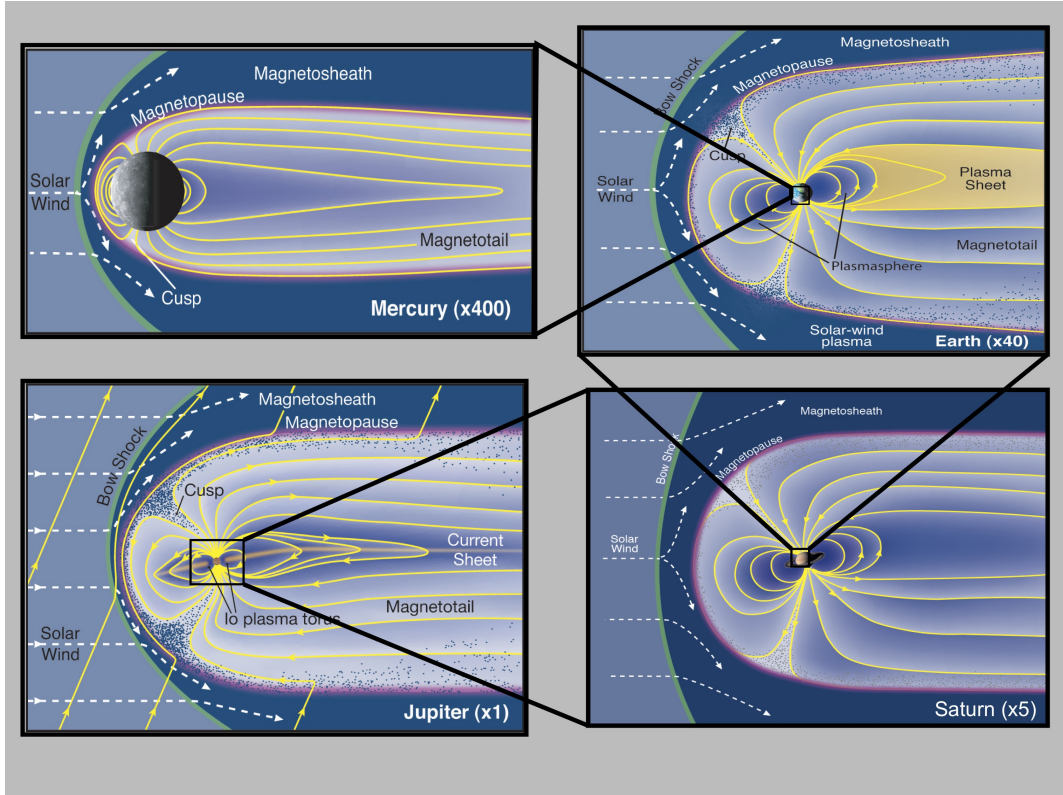


Figure 1.3: Diagram comparing the relative sizes and shapes of the magnetospheres of Mercury, Earth, Jupiter and Saturn, from Fran Bagenal and Steve Bartlett at LASP.

field. Table 1.1 provides some typical parameters for the planets Earth, Jupiter and Saturn that help illustrate this. For example, the Jovian planetary dipole magnetic moment is some 20,000 times greater than that of Earth, with correspondingly higher magnetic field strength. This therefore means a much greater magnetic pressure inside Jupiter's magnetosphere. In addition, the solar wind dynamic pressure D_{P} is defined by

$$D_{\text{P}} = \rho_{\text{m}} u_{\text{SW}}^2 \quad (1.22)$$

where ρ_{m} is the mass density of the solar wind and u_{SW} is the velocity. As discussed in Section 1.2, ρ_{m} falls approximately as r^{-2} while u_{SW} remains approximately constant, and so the external solar wind dynamic pressure is much lower for the planets in the outer solar system, falling as approximately r^{-2} .

This pressure-balance relationship is reflected in the ‘dipole stand-off distance’ R_{CF} for each planet given in Table 1.1, where CF stands for the derivation by ?. This distance is a theoretical location of the magnetopause, measured from the planet centre to the sub-solar point on the magnetopause surface, which would be

Table 1.1: Comparison of typical magnetospheric parameters for Earth, Jupiter and Saturn, adapted from ? and references therein. $1\text{ AU} = 1.496 \times 10^8 \text{ km}$ and $1\text{ M}_{\text{EARTH}} = 7.9 \times 10^{15} \text{ Tm}^3$.

	Earth	Jupiter	Saturn
Planet radius R_P (km)	6371	71 492	60 268
Distance from Sun (AU)	1	5.2	9.6
Solar wind number density (cm^{-3})	7	0.2	0.07
Spin period (hr)	24	9.9	10.6
Magnetic moment (M_{EARTH})	1	20 000	600
Equatorial surface magnetic field (nT)	30 600	430 000	21 400
Dipole stand-off distance R_{CF} (R_P)	$10 R_E$	$46 R_J$	$20 R_S$
Observed stand-off distance R_{MP} (R_P)	$8 - 12 R_E$	$63 - 92 R_J$	$22 - 27 R_S$

expected if the external solar wind dynamic pressure was balanced exactly by the magnetic pressure associated only with an internal *dipole* magnetic field. We can see that it is much greater for Jupiter and Saturn than for Earth, as expected from the pressure-balance explanation just given.

However, at Saturn and Jupiter in particular, the observed magnetopause stand-off distances are significantly larger even than the Chapman-Ferraro estimates. This is mainly due to the significant internal plasma sources at each planet. At Saturn, the icy moon Enceladus orbits at a distance of $3.95 R_S$, (where R_S is the radius of Saturn, 60 268 km) and ejects water group molecules into the magnetosphere at a rate of $\sim 150 \text{ kgs}^{-1}$ (?). At Jupiter, the volcanic moon Io orbits at $5.9 R_J$ (where R_J is the radius of Jupiter, 71 492 km) and ejects sulphur dioxide into the magnetosphere at $\sim 1000 \text{ kgs}^{-1}$ (?). At each planet, this material is partially ionised, forming a torus of plasma around each planet. The plasma pressure associated with this population adds to the internal magnetic pressure, inflating the magnetosphere beyond the predictions of a vacuum a dipolar internal field model. This is discussed in more detail in Section 1.4.2. In contrast at Earth, the Moon does not contribute a significant plasma population, and also mainly orbits the planet beyond the magnetosphere boundary, and thus does not have the same degree of influence on Earth's magnetosphere (e.g. ?).

For Jupiter and Saturn, these internal plasma populations not only influence the overall size of the magnetosphere but also the internal structure of the magnetic field. This is due to the rapid rotation rates of the two planets, shown by the short spin periods in Table 1.1. Due to the aforementioned frozen-in field theorem, the mag-

netospheric plasma is azimuthally accelerated towards co-rotation with the rapidly rotating magnetic field of the magnetosphere. The centrifugal force associated with this rotation confines the plasma towards the rotational equator, creating a plasma sheet. In order to balance this centrifugal force, the magnetic field is distorted about the plasma sheet from a dipolar magnetic field into a disc-like *magnetodisc* structure, with a strong associated magnetic curvature force. This structure is characterised by field lines that are stretched radially outwards near the equatorial plane in the outer magnetosphere (as can be seen particularly for Jupiter in Figure 1.3), and is supported by the azimuthal ring current. The intensity of the ring current is enhanced by a population of hotter, more variable plasma that originates in the outer magnetosphere at both Saturn (e.g. ?) and Jupiter (e.g. ?), with observed plasma β of the order 2–5 and ~ 100 for these populations respectively. The magnetic field strength of the magnetodisc field structure in general varies more slowly with radial distance in the outer magnetosphere than a dipolar magnetic field, and thus also significantly influences pressure balance at the magnetopause. This behaviour is investigated for both Saturn and Jupiter in Chapter ??.

1.3.3 Magnetospheric Dynamics

The simplest dynamical process that a magnetosphere undergoes is compression and expansion under varying solar wind conditions. For example, as the local solar wind dynamic pressure increases, due to an increase in velocity or number density by some process as described in Section 1.2, the magnetosphere becomes compressed. This compression causes the internal magnetic field pressure to increase, until (for steady state conditions) it balances the enhanced external solar wind dynamic pressure and a new equilibrium magnetopause location is reached. If the solar wind pressure decreases, the magnetosphere then inflates. The magnetopause is therefore in constant motion, with a velocity of order 10 kms^{-1} at Earth (?) and 100 kms^{-1} at Saturn (?). The exact response of the magnetosphere to varying D_P varies significantly between planets due to the different internal structures. For Saturn in particular, the distance that the magnetopause location shifts for a given change in D_P , and how this varies with different internal and external conditions, is the subject of the study in Chapter ??, and is discussed in detail there.

However, even under approximately constant solar wind conditions, a magne-

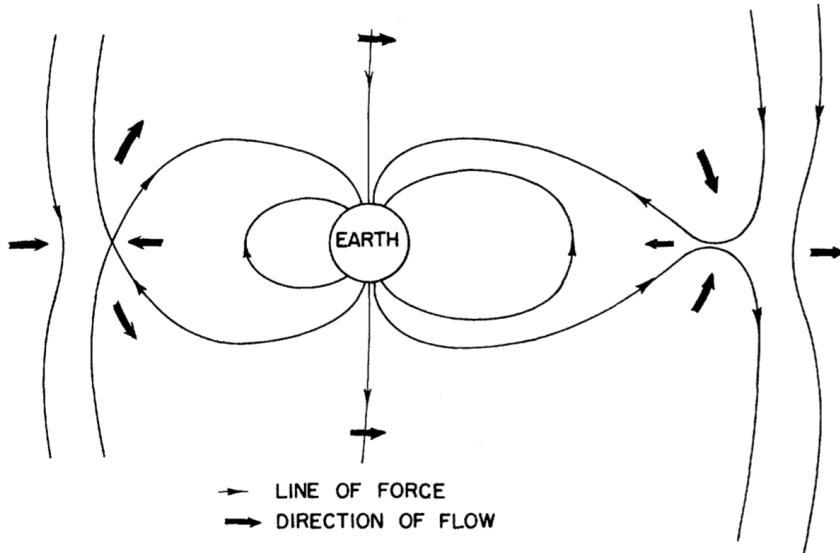


Figure 1.4: Diagram showing the Dungey Cycle process at Earth, from ?. Thin black ‘lines of force’ are magnetic field lines. The solar wind flows from left to right.

tosphere is not a static object. At the ‘solar-wind driven’ magnetospheres of Earth and Mercury, the dominant large-scale dynamic process is known as the *Dungey Cycle*, after ?. A diagram of this process is shown in Figure 1.4. For an IMF oriented anti-parallel to the planetary magnetic field, conditions are favourable for reconnection of the two magnetic fields at the dayside magnetopause, as the magnetic field varies on small spatial scales across the magnetopause boundary (as discussed in Section 1.1.3). The planetary magnetic field lines are then open to the solar wind at one end whilst still anchored to the planet at the other, and are thus convected by the solar wind flow downstream to the nightside. This leads to a build-up of magnetic flux on field lines in the magnetotail, which then reconnect across the tail current sheet. This causes plasma to accelerate and return on closed field lines back towards the planet on the nightside. At Earth, this process is associated with the generation of aurora along the boundary between open and closed magnetic field lines, in the northern and southern polar atmospheres (e.g. ?). As the energetic electrons in the plasma gyrate around the polar magnetic field lines and move towards the planet, they excite atoms in the atmosphere, which then decay back to their lower energy levels and emit photons in the process. These are observed which are observed as auroral emissions.

At Jupiter and Saturn, the dominant dynamical process which causes a large-

scale reconfiguration of the magnetic field is internally driven by the rapid planetary rotation, and thus we say they are ‘rotationally driven’ magnetospheres. This process is known as the Vasyliunas cycle, after ?, and a diagram depicting it is shown in Figure 1.5. As discussed in the previous section, these rapidly rotating magnetospheres have significant internal plasma populations, which are accelerated to near-corotation with the rotating planetary magnetic field. The centrifugal interchange instability causes this plasma to be transported radially outwards, such that inner cold, dense flux tubes are exchanged with outer hot, tenuous flux tubes (?), and the magnetic field is stretched out as shown in region 1 of Figure 1.5. As the flux tubes rotate around to the nightside, they are no longer as confined by the magnetopause boundary and so expand down the tail, and the magnetic field becomes increasingly more stretched (region 2) until reconnection occurs across the tailward portion of the flux tube (region 3). This generates the release of a *plasmoid* down the tail, and the newly empty flux tube is then convected back around the planet via the dawn side.

This cycle is dominant over the Dungey cycle for the outer giant planets due to the combined effects of the much faster rotation rates, and overall larger magnetospheric sizes, which means a much longer period of time for a magnetic field line to be convected across the polar cap from dayside to nightside (?). However at Saturn in particular, it still uncertain how much of a role the Dungey cycle has to play (e.g. ?). In particular, Saturn’s aurora are thought to have an ‘Earth-like’ origin, associated with flow shear at the boundary between open and closed magnetic field lines. We discuss this further in Chapter ??.

In addition to these main modes of plasma transport in planetary magnetospheres, there are also numerous small-scale dynamical processes, such as Kelvin-Helmholtz vortices on the magnetopause surface; however these vary significantly between planets and are not relevant to the work of this thesis, and so we do not cover them explicitly here.

1.4 Saturn and its Magnetosphere

Saturn orbits the Sun once every \sim 29 years, on an elliptical orbit at an average distance of 9.6 AU. Saturn is approximately 10 times the size of Earth (by radius), and around 100 times as massive, meaning its density is around 1/10 of Earth’s. This

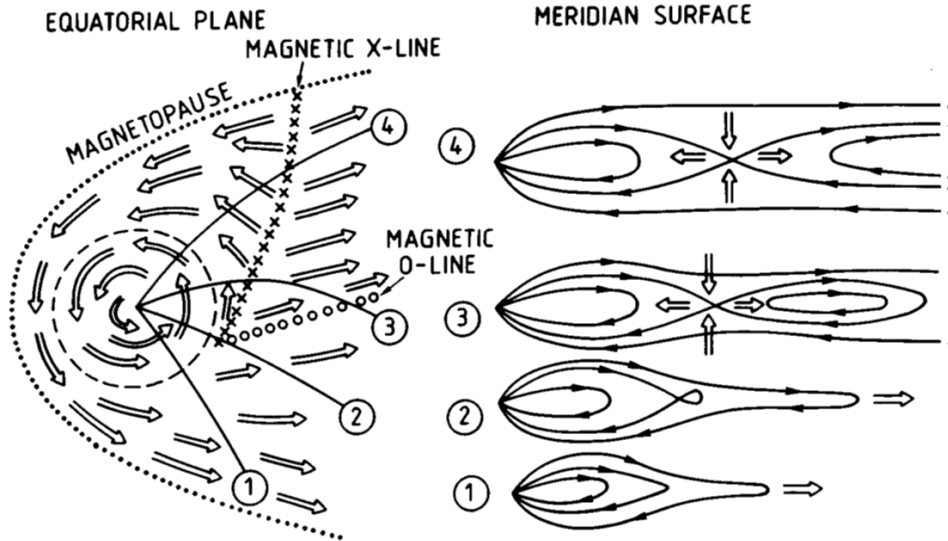


Figure 1.5: Diagram showing the Vasyliunas cycle of plasma transport, from ?. The dotted line shows the magnetopause boundary, the dashed line shows the region where plasma perfectly corotates with the magnetic field, and empty arrows show the plasma flow direction.

is because Saturn is a ‘gas giant’ planet, composed mainly of molecular hydrogen and helium, with a small rocky core. Between the core and the outer layers, the hydrogen is compressed to such high pressures and temperatures that it becomes ‘metallic’, flowing and conducting electricity and generating the dynamo of Saturn’s planetary magnetic field.

The internal planetary magnetic field is approximately dipolar, though with smaller higher order moments. It may be approximated by a dipole offset northwards from the planetary equator by $\sim 0.05 R_S$ (?). Arguably the most interesting aspect of Saturn’s internal magnetic field is that the dipole axis is extremely closely aligned with the planet spin axis, with the same study by ? finding an upper limit of 0.01° difference between them. This is seemingly in contradiction with Cowling’s Theorem, which states that an active dynamo cannot maintain a perfectly axisymmetric magnetic field (?). This extreme axisymmetry also means it is nearly impossible to determine the rotation rate of the planet’s deep interior from magnetic field measurements; however, a range of periodic phenomena are observed at Saturn, at periods assumed *close* to the true planetary rotation rate, as discussed in detail in Section 1.4.1.

From Table 1.1 and the associated discussion, we have seen that in many ways Saturn’s magnetosphere is an intermediate case between Earth and Jupiter. It is

therefore a particularly interesting system to study, and can be used to learn more about magnetospheric physics in a global context. Saturn's magnetosphere was first investigated *in situ* with single flybys by the outer solar system space missions *Pioneer* (1979), *Voyager 1* (1980) and *Voyager 2* (1981). These observations did not reveal a significant magnetodisc magnetic field structure on Saturn's dayside (as was known to exist at Jupiter), although did provide some evidence for a thin current sheet on the dawn flank (?). However with the arrival of the *Cassini* space mission into orbit around Saturn in 2004, and its continued observation of the system until late 2017, our scientific understanding of Saturn's magnetosphere has been revolutionised. (The *Cassini* space mission is discussed in detail in Chapter ??.)

We now know that in the outer magnetosphere, a non-negligible magnetodisc magnetic field structure typically exists at all local times beyond a radial distance of $\sim 15 R_S$, due to the reasoning discussed in Section 1.3.2. However particularly on the dayside near noon, it was found that a significant magnetodisc structure only forms under relatively low solar wind dynamic pressure, where the subsolar magnetopause stand-off distance becomes greater than $\sim 23 R_S$. When the magnetosphere is more compressed than this, the magnetic field near noon is approximately dipolar (?). A study by ? based on ring-current modelling found similar behaviour. It is interesting that this threshold value of $\sim 23 R_S$ falls between the two modes of the bimodal distribution in magnetopause stand-off distances observed by ? and ?, of $21 R_S$ and $27 R_S$. This transition between a dipolar and disc-like field is broadly due to overall force balance in Saturn's magnetosphere; for a more expanded system, the magnetic field strength is weaker in the outer magnetosphere, and so a larger magnetic tension force (i.e. a more curved field line structure) is needed to balance the centrifugal and plasma pressure gradient forces acting radially outwards on the plasma. In Chapter ?? of this thesis, we present theoretical results that show the compressibility of the magnetosphere also changes behaviour at around this value of stand-off distance, at $\sim 25 R_S$.

The formation of a magnetodisc structure at Saturn is also influenced by the variable hot plasma population observed by ? and others, as discussed in Section 1.3.2, through an enhancement of the equatorial ring current intensity. By consideration of Ampère's law, it can be understood that the magnetic field asso-

ciated with an azimuthal current flowing in the direction of corotation decreases Saturn’s planetary magnetic field in the inner magnetosphere, and increases it in the outer magnetosphere. This is an important aspect of a magnetodisc magnetic field structure. Many studies have attempted to characterise the thickness and radial extent of this equatorial ring current, using a combination of *Cassini* data, and models such as that of ??, which assumes an azimuthally symmetric current loop of uniform thickness and rectangular cross section. The nature of the ring current has been observed to vary significantly over time, with location, and with system size (e.g. ?), with a variable half-thickness of average $\sim 1.5 R_S$ and significant radial extent, from around $7 R_S$ out to around $18 R_S$, at times reaching the magnetopause boundary on the dayside (e.g. ??). However due to incomplete coverage across local time for most of the *Cassini* mission, it was not until near the end of the mission that the local time asymmetry of the ring current was demonstrated by ?. Indeed, the local time variation in the large scale structure of Saturn’s magnetosphere is still not fully understood, and is studied and characterised further in this thesis in Chapter ??, using a flexible model of the ring current adapted from ?, known as the UCL/AGA model. This model is discussed in Section 1.5.

1.4.1 Near-Planetary Period Periodicities in Saturn’s Magnetosphere

Another key aspect of Saturn’s magnetosphere that is still not fully understood, is the nature of the observed periodic variations in field and particle properties. These variations, summarised in ?, have periods ranging from around 10.6-10.8 hours, assumed close to the true planetary rotation rate. Magnetospheric periodicities have been found in the location of the auroral oval (?), and the magnetopause boundary (?); the magnetic field strength and direction (??); electron densities (?); ion distributions (?); and energetic neutral atoms (?). These observations are especially interesting due to the aforementioned axisymmetry of Saturn’s magnetic field, which means they cannot be adequately explained by a geometric tilt of the magnetic field. In addition, some of the observed periods vary relatively quickly, by up to 1% over the course of a year, and thus cannot be associated with changes to the planet’s deep interior. This complex behaviour is apparently unique to Saturn, and has made it impossible directly to measure Saturn’s true ‘core’ rotation rate.

Initially, periodicities in radio observations of Saturn’s auroral regions from the *Voyager* spacecraft suggested a planetary rotation period of 10.657 h (?). This radio emission is known as Saturn Kilometric Radiation, or SKR. However observations from the *Ulysses* (?) and later *Cassini* (?) missions revealed that the SKR period was actually drifting over time, and thus could not be associated with the core rotation rate. A reanalysis of magnetometer data from the *Voyager* and *Pioneer* missions then showed a similar periodic behaviour in the magnetic field. This led to the development of a ‘camshaft’ model, where a rotating equatorial magnetic anomaly that is fixed in longitude triggers radial waves that cause the observed perturbations (?). To further complicate the picture, two distinct periods were then discovered in the SKR signal by *Cassini*, associated separately with the Northern and Southern hemispheres (?). This phenomenon was then also observed in more recent *Cassini* magnetic field observations (e.g. ??). In these and other studies, such as ?, a picture has now been developed of how these hemispheric magnetic perturbations are generated, by two large-scale field-aligned current systems that rotate at slightly different rates in each hemisphere. The magnetic field associated with each current system is dominant in the respective hemisphere, and can be approximated in the outer magnetosphere by a rotating, transverse oriented dipole. However the true magnetic field perturbation is much more complex, and is currently an area of active research, with some final *Cassini* results still to be fully analysed. The physical origins of these current systems are also still not fully understood, but are thought to be associated with twin atmospheric vortices flowing in the polar upper atmosphere/ionosphere in each hemisphere (???).

In the equatorial plane, these magnetic field perturbations have the effect of making Saturn’s current sheet appear to ‘flap’ above and below the rotational equator once per planetary rotation (e.g. ?). Similar behaviour is also observed at Jupiter. However at Jupiter the dipole axis is tilted 9.4° relative to its rotation axis, which means that relative to the rotational equator, the current sheet behaves approximately as a rotating, tilted disc, and so this behaviour is expected. In addition, at Saturn, these periodic magnetic field perturbations also have the effect of periodically thickening and thinning the current sheet at different longitudes (?), associated with a large scale compression and expansion of the magnetosphere in a given region,

known as ‘breathing’ (?). Both the ‘flapping’ and ‘breathing’ behaviours are controlled by the relative phases of the northern and southern magnetic perturbations, noting that their independent rotation rates cause the phase relationship between them to change over time, known as beating. This complicated dynamical behaviour is the focus of much current research, and is the subject of the study in Chapter ??.

1.4.2 Pressure Balance at Saturn;s Magnetopause

As previously mentioned, the magnetopause boundary can be approximated as the location where the effective pressure of the solar wind exerted on the magnetosphere is exactly balanced by the sum of the internal magnetospheric particle and field pressures.

Before impacting on the magnetopause, the solar wind flow is first decelerated via the bow shock, and is deflected around the magnetosphere obstacle. This acts to reduce the dynamic pressure incident on the magnetopause surface, and must be accounted for when considering pressure balance. ? used Bernoulli’s equation in combination with the Rankine-Hugoniot jump conditions across the bow shock, assuming adiabatic flow of the solar wind, to show that the relation

$$\frac{B_{\text{MS}}^2}{2\mu_0} + P_{\text{MS}} = kD_P \cos^2 \psi + P_0 \sin^2 \psi \quad (1.23)$$

provides an approximation that is valid across the magnetopause surface, not just at the nose. For clarity the subscript MS denotes magnetospheric properties, such that the terms on the left hand side of equation 1.23 are the magnetospheric magnetic and plasma pressures respectively. ψ is the flaring angle measured between the upstream flow velocity vector and the normal to the magnetopause surface, such that $\psi = 0$ at the nose and generally increases as you move anti-sunward along the magnetopause surface. The first term on the right hand side is associated with the solar wind dynamic pressure, where k is a positive constant ≤ 1 to account for the aforementioned diversion of flow, and the $\cos^2 \psi$ factor accounts for the reduction in the normal component of dynamic pressure on the flanks and tail of the magnetosphere. The second term on the right hand side is composed of a ‘static’ pressure P_0 associated with the thermal pressure of the solar wind, and a $\sin^2 \psi$ factor to ensure a real (i.e. not imaginary) flow velocity in the subsolar region (see

?).

In order to improve agreement with the results of MHD simulations from ?, and to improve the consistency of D_P estimates, ? proposed a modification to this relation such that P_0 is dependent on D_P . The relationship then becomes

$$\frac{B_{\text{MS}}^2}{2\mu_0} + P_{\text{MS}} = \left[k \cos^2(\psi) + \frac{k_B T_{\text{SW}}}{1.16 m_p u_{\text{SW}}^2} \sin^2(\psi) \right] D_P \quad (1.24)$$

where k_B is the Boltzmann constant, m_p is the mass of a proton, and T_{SW} and u_{SW} are the solar wind temperature and velocity respectively. The value of k depends on the ratio of specific heats γ in the solar wind, and the upstream sonic Mach number M . For high ($\gtrsim 8$) Mach number flow with $\gamma = 5/3$, $k = 0.881$ (?), which is a valid assumption for the solar wind at Saturn’s orbit (e.g. ??). In ?, the authors use values of $k_B T_{\text{SW}} = 100 \text{ eV}$ and $u_{\text{SW}} = 460 \text{ km s}^{-1}$ to represent typical solar wind conditions at Saturn; we use the same values in this thesis when we utilise this relation.

This relation allows an approximation of the solar wind dynamic pressure to be made, when only internal information about the state of the magnetosphere is known. Thus this relation is often used in studies that attempt to model the shape and size of the magnetopause boundary in response to changing D_P , using only *in situ* Cassini data for the magnetic and plasma pressure inside the magnetosphere. These studies are discussed in more detail in Chapter ??.

1.5 The UCL/AGA Force-Balance Model of Saturn’s Magnetodisc

Throughout this thesis we will employ the University College London/Achilleos-Guio-Arridge (UCL/AGA) magnetodisc model from ??, with appropriate modifications as described in each chapter. This model is based on a magnetic field and plasma model originally constructed for the Jovian magnetodisc by ?, and adapted for the Saturn system. More information can be found in ?. The model is axisymmetric about the planetary dipole/rotation axis, which are assumed to be parallel. This parallel assumption is appropriate for Saturn in particular, as the rotation and dipole axes are aligned to within 0.01° (?). This axisymmetric assumption is appropriate as an approximation of the large-scale structure of the magnetic field,

as shown by ?, who compared the gradients of currents in radial, azimuthal and meridional directions and found the azimuthal gradients could be neglected. It is constructed based on the assumption of force balance in the rotating plasma of the magnetosphere between the Lorentz body force (including magnetic pressure and tension forces), pressure gradient force and centrifugal force, such that

$$\mathbf{J} \times \mathbf{B} = \nabla P - nm_i\omega^2\rho\hat{\mathbf{p}} \quad (1.25)$$

where ρ is cylindrical radial distance from the axis, with $\hat{\mathbf{p}}$ its unit vector. The plasma properties are isotropic pressure P , temperature T , ion number density n , mean ion mass m_i and angular velocity ω . Note that this construction is equivalent to equation 1.12, the MHD momentum equation, with simplifying assumptions as described in that section, assuming force balance such that the acceleration of the plasma is zero, and including the centrifugal force on the plasma associated with the planetary rotation, for a frame of reference that corotates with the plasma.

As a consequence of Maxwell's equation 1.4, any magnetic field can be presented in terms of two Euler potentials α and ξ , such that

$$\mathbf{B} = \nabla\alpha \times \nabla\xi. \quad (1.26)$$

For an axisymmetric field with no azimuthal component, the forms of α and ξ can be chosen such that all the information about the poloidal magnetic field is contained in one Euler potential which we call $\alpha = \alpha(r, \mu)$, where r is radial distance from the origin, and $\mu = \cos\theta$, the cosine of colatitude. Using this form of α , ? demonstrated that equation 1.25 is equivalent to the partial differential equation

$$\frac{\partial^2\alpha}{\partial r^2} + \frac{1-\mu^2}{r^2}\frac{\partial^2\alpha}{\partial\mu^2} = -g(r, \mu, \alpha) \quad (1.27)$$

in normalised units, where $g(r, \mu, \alpha)$ is a source function determined by the distribution of plasma and angular velocity in r, μ space. This equation can be solved semi-analytically using Jacobi polynomials as laid out in detail in ?, Appendix to give surfaces of constant α , corresponding to magnetic field lines, in r, μ space. The model solution also provides a prediction of the local plasma pressure, and the az-

imuthal current density components associated with each of the terms on the right hand side of equation 1.25.

Since the source function is itself dependent on α , equation 1.27 must be solved iteratively, starting from a pure dipole magnetic field and then successively perturbing it. At each iteration, a linear combination of the present solution α_i and the previous solution α_{i-1} is used as input for the next iteration calculation, such that

$$\alpha_{i+1(\text{input})} = \gamma\alpha_i + (1 - \gamma)\alpha_{i-1}, \quad (1.28)$$

where $\gamma < 1$ controls the relative weighting between the previous and current solutions. This is a form of numerical relaxation which stabilises the approach to the equilibrium solution. This $\alpha_{i+1(\text{input})}$ is then used to calculate the source function in equation 1.27 to solve for α_{i+1} . In the original model construction, the two components were weighted equally ($\gamma = 0.5$) and calculations continued until the maximum relative difference between successive iterations fell below a chosen ‘tolerance’ $\delta = 0.5\%$, considered as convergence. In some of the work in this thesis we found that, for models with more extreme input parameters, it was necessary to weight the previous solution up to nine times more heavily than the present solution ($\gamma = 0.1$), in order to achieve convergence. (Exactly what constitutes an ‘extreme parameter’ will be discussed in future chapters.) In order to keep the ratio δ/γ constant at 10^{-2} , and therefore consistent with the original model approach, this corresponds to using a more stringent stopping tolerance $\delta = 10^{-2} \times 0.1 = 0.1\%$ in such cases.

The global plasma properties can then be inferred entirely from the calculated magnetic field structure, using appropriate boundary conditions, as follows. ? explained that as a consequence of equation 1.25, with T and ω constant along magnetic field lines (according to Liouville’s theorem and Ferraro’s isorotation theorem respectively), the plasma pressure P is determined by

$$P = P_0 \exp \left(\frac{\rho^2 - \rho_0^2}{2\ell^2} \right), \quad (1.29)$$

where ℓ is the *confinement scalelength* (in ρ)

$$\ell^2 = \frac{2k_B T}{m_i \omega^2}. \quad (1.30)$$

The subscript 0 means the quantity evaluated at the equatorial crossing point of the magnetic field line. This represents the plasma being confined towards the rotational equatorial plane due to the centrifugal force exerted on it. Again, this is in normalised units as described in ?, and thus ℓ is in units of R_S here. The model assumes that the plasma is composed of a cold and hot population; for the hot plasma population, the thermal energy associated with the plasma is significantly greater than the centrifugal potential, and so ℓ^2 tends to infinity, such that the hot plasma pressure is not confined to the equator but is constant along magnetic field lines, $P_H = P_{H0}$. This assumption is supported by observations such as ?, who used data from the *Cassini* MIMI instrument to show that the hot plasma population extends to high latitudes, particularly on the dayside, verifying that the plasma can effectively fill their flux tubes due to their high energies. Similarly, a recent study by ? showed that the UCL/AGA model with this assumption accurately predicts the relationship between high latitude and equatorial hot plasma pressure distributions. Hence, the full form of equation 1.29 is only necessary for calculating the cold plasma pressure.

The requisite boundary conditions for the model are, then, the equatorial radial profiles of the relevant plasma properties. These were obtained from studies using results mainly from *Cassini* plasma instruments CAPS and MIMI/INCA, as summarized in ?, and updated in ?. For the cold plasma population, the profiles for m_i and T were obtained from ?, ω profiles from ? and ?, and the flux tube content information from ?. For the studies described in Chapters ?? and ?? we updated some of these boundary conditions using more recent results from ?, as described in those chapters, with details in the Appendix ??.

As the hot plasma pressure is assumed uniform along magnetic field lines, the plasma population may be completely characterised by a particular equatorial plasma pressure P_{H0} and flux tube volume V per unit of magnetic flux, where

$$V = \int_0^{s_B} ds/B, \quad (1.31)$$

and ds is an element of arc length along the magnetic field line. The integral limits represent measurement along a field line of total length s_B between the southern and northern ionospheric footprints at $1 R_S$. The flux tube volume is therefore dependent on both the shape of magnetic field lines, via ds , and the strength of the field, via B . Studies using *Cassini* MIMI data such as ? found that the equatorial pressure associated with the hot plasma population was highly variable with ρ and over time, as described in Section 1.4. In light of these observations, the original ? model simply parameterised the global hot plasma content by a single ‘hot plasma index’ K_H , where $K_H = P_{H0}V$ is constant beyond $8 R_S$, and P_{H0} decreases linearly to 0 inside that distance. A similar parameterisation, though with different values of the constants, was made in ?, who argued that for the Jovian system, under the expected conditions of rapid radial diffusion, the hot plasma would be transported isothermally. In ? the authors used a value of $K_H = 2 \times 10^6 \text{ Pa m T}^{-1}$ to represent just above ‘typical’ hot plasma content conditions at Saturn, although results presented in that study suggest K_H may vary in the range $10^5\text{--}10^7 \text{ Pa m T}^{-1}$. Parameterising the hot plasma content in this way provides the flexibility to very simply characterize the level of ring current activity in the model, and thus investigate the effect of the varying hot plasma content on magnetospheric structure, and magnetospheric compressibility. This is the basis of the study described in Chapter ???. In this chapter we also discuss some of the s of modifying the definition of K_H to correspond to adiabatic plasma transport. In Chapter ???, this hot plasma pressure boundary condition is updated to describe different local time sectors, using recent results from ?.

Finally, at every iteration, a small, uniform, southward-directed ‘shielding field’ is added to the magnetic field, in order to approximately account for the magnetic field associated with the magnetopause and magnetotail current sheets. Sketches of these current systems are included in the diagram in Figure 1.2, though note they are in the opposite sense for the Saturn system due to the opposite orientation of Saturn’s planetary dipole. In ? the magnitude of this field was chosen by calculating dayside equatorial averages of the empirical field models of ? and ?, and it varied with model magnetodisc radius R_D (see ?, Figure 6). In particular the component of the shielding field associated with the magnetopause currents was based on a dipole

approximation of the magnetospheric magnetic field. In Chapter ?? we update this calculation for a more realistic magnetodisc magnetic field, and in Chapter ?? we modify this calculation using local time sector averages of the models of ? and ?, to account for the increased significance of the tail current field compared to the magnetopause current field for nightside local time sectors.

Outputs from the UCL/AGA magnetodisc model for two configurations are shown in Figure 1.6, calculated with magnetopause radii $21 R_S$ and $27 R_S$ respectively, in line with the previously mentioned bimodal distribution in magnetopause stand-off distances observed by ?. In both models we use $K_H = 1 \times 10^6 \text{ Pa m T}^{-1}$ to represent typical conditions at Saturn. The top and middle panels show the distribution of hot plasma pressure; as this quantity is constant along magnetic field lines, colour contours exactly reveal the magnetic field structure in the models. The bottom panel shows the equatorial profiles of total magnetic field strength for each model, compared to a dipole magnetic field. This figure shows how the UCL/AGA model predicts a more disc-like magnetic field structure, with more radially stretched field lines particularly in the middle magnetosphere, for a more expanded system, as is expected from discussions in Section 1.4. The same information for a more expanded and wider range of system sizes is shown in Figure ?? in Chapter ??, following adaptations and parameterisations discussed in that chapter.

1.6 Open Questions about Saturn’s Magnetosphere: Motivations and Summary of this Thesis

As a community, we are still trying to understand the large-scale structure of Saturn’s magnetosphere, and how it varies in response to internal and external influences. We know that the rapid planetary rotation rate, significant internal hot and cold plasma populations, and external solar wind conditions all play a role in determining the configuration of the magnetosphere – but which factor is dominant, and does this relationship change under different conditions and in different places?

The answers to these questions have consequences for other areas of magnetospheric physics at Saturn. In Sections 1.3.2 and 1.4.2 we touched on the concept of magnetospheric compressibility, and how the size of the magnetosphere scales with varying solar wind dynamic pressure. From equation 1.24, it can be seen that the

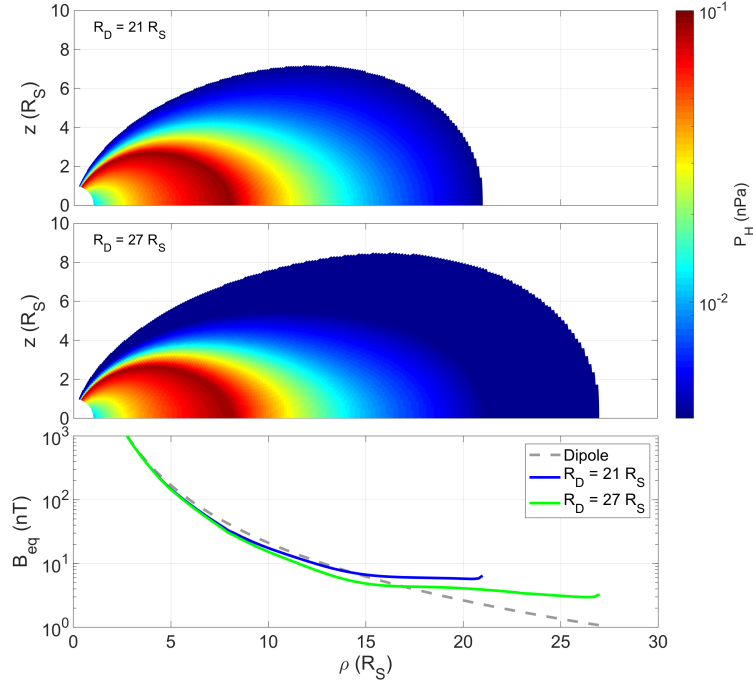


Figure 1.6: (a,b) Hot plasma pressure P_H predicted by the UCL/AGA magnetodisc model for models with different disc radii R_D , as a function of cylindrical coordinates ρ and z , shown on a colour scale as per the colourbar. (c) Radial profiles of equatorial magnetic field strength for each of the two models, as shown by the legend, with dipole magnetic field profile shown by the grey dashed line for comparison.

relative magnitudes of the magnetic and plasma pressures just inside the magnetopause are important in determining this pressure balance, and hence the system size. Therefore an investigation of the magnetospheric compressibility, and how it varies under different conditions, can reveal information about overall pressure balance within the magnetosphere. In Chapter ?? we investigate this compressibility using the ? magnetodisc model calculated at different system sizes. This approach complements previous observational studies based on *Cassini* data, and also provides an opportunity to explicitly investigate the influence of the variable hot plasma population on the compressibility behaviour. We also use our results to make a direct comparison with the compressibility of Jupiter's magnetosphere, to test our expectations that Saturn behaves as an intermediate between Earth and Jupiter.

The structure of Saturn's magnetodisc, and in particular the equatorial current sheet, also has consequences for understanding the periodic perturbations in Saturn's magnetic field. We discussed in Section 1.4.1 how Saturn's current sheet

is observed to both ‘flap’ and ‘breathe’ periodically, at approximately the planetary rotation rate, due to rotating hemispheric magnetic perturbations. However this complicated behaviour is still not fully understood, and research is ongoing in the community using both *Cassini* data analysis and MHD modelling approaches. In Chapter ?? we attempt to model these two periodic behaviours simultaneously, using the ? magnetodisc model at different sizes to characterise the configuration of the magnetodisc at different phases of the planetary rotation. This allows us to provide an insight into how the breathing behaviour manifests in the *Cassini* magnetic field observations, and utilises the knowledge gained in the previous chapter of this thesis, about how magnetospheric structure varies with system size. In addition for the flapping motion, we use a geometric model of a tilted and rippled current sheet and fit the combined model to *Cassini* magnetic field observations, in order to investigate how the behaviour varies over time and under different conditions.

We still do not have a complete picture of how the large-scale structure of Saturn’s magnetosphere varies across magnetic local time. In particular the dawn/dusk asymmetry in the magnetic field configuration is not well constrained. This is in part due to relatively poor sampling of the dawn sector near the equator for much of the *Cassini* space mission, and the generally smaller scale asymmetries between the two sectors compared to noon/night, although recent results from MHD simulations have provided some insights (e.g. ?). It is important to investigate local time asymmetry in the magnetospheric magnetic field structure as this has consequences for other magnetic phenomena at Saturn, such as the location of the main auroral oval, and the aforementioned periodic modulation in the current sheet thickness. Therefore in Chapter ?? we investigate this local time variation using a version of the ? model to characterise four different local time sectors, using more recent *Cassini* observations as boundary conditions to improve our characterisation of local times beyond noon.

Finally, in Chapter 2 we summarise the key results of the work presented in this thesis, and suggest avenues for future research that can best utilise these results, in order to continue our pursuit of understanding the configuration of Saturn’s magnetosphere.

But first, we must discuss in more depth the other tool we use to investigate

Saturn’s magnetosphere; the *Cassini* space mission to Saturn.

Chapter 2

Local Time Variation in Large-Scale Structure of Saturn's Magnetosphere

Throughout this thesis, we have shown how the large-scale structure of Saturn's magnetosphere is determined by internal and external factors, including the rapid planetary rotation rate, significant internal hot and cold plasma sources, and varying solar wind pressure. However it is still not fully understood which factors dominantly influence the configuration of the magnetosphere, and in particular how this relationship varies with local time. In this chapter, we explore this in detail using the UCL/AGA model Saturn's magnetodisc to describe the magnetosphere at different local time sectors. For model inputs, we use recent observational results which suggest a significant local time asymmetry in the pressure of the hot plasma population, and magnetopause location. We make calculations under different solar wind conditions, in order to investigate how these local time asymmetries influence magnetospheric structure for different system sizes. We find significant day/night asymmetries in the model magnetic field, consistent with recent empirical studies based on *Cassini* magnetometer observations. We also find dawn-dusk asymmetries in equatorial current sheet thickness, with the varying hot plasma content and magnetodisc radius having comparable influence on overall structure, depending on external conditions. We also find significant variations in magnetic mapping between the ionosphere and equatorial disc, and ring current intensity, with substantial enhancements in the night and dusk sectors. These results have consequences for interpreting many magnetospheric phenomena that vary with local time, such as reconnection events and auroral observations. The contents of this chapter are heavily

based on the study by ?, submitted.

2.1 Introduction

In recent years, a more global understanding of Saturn’s magnetosphere has become possible largely thanks to the extensive temporal, spatial and seasonal coverage of the *Cassini* space mission. *Cassini* toured the Saturnian magnetosphere from 2004 to 2017, and is described in detail in Chapter ???. In particular, there is now an opportunity to investigate in more detail how the large-scale structure of Saturn’s magnetosphere varies with *local time*, and which factors control this behaviour. This information is important for interpreting a range of phenomena at Saturn; for example the likelihood of reconnection events in different regions of the magnetosphere (?), which is related to how current sheet thickness varies with local time (?). Understanding more about the structure of the current sheet is also important for studies of the observed periodicities at Saturn’s magnetosphere, which investigate how the position and thickness of the equatorial current sheet appear to be modulated at a period close to the planetary rotation rate (e.g. ?), and the study we presented in Chapter ???. More generally, a good picture of the global magnetic field structure at different local times is important for understanding how different regions of the magnetosphere magnetically map to the polar ionosphere in different local time sectors, for example when interpreting observations of Saturn’s aurora. For example, the recently published empirical magnetic field model by ? suggests significant day-night asymmetry in equatorial-ionospheric magnetic mapping profiles, and local time asymmetries in the location of Saturn’s aurora have been observed in studies such as ??.

A recent empirical study of magnetopause crossings by ? showed evidence of a dawn-dusk asymmetry in the typical location of the magnetopause boundary, with in general a larger magnetopause radius on the dawn flank. In addition, a survey of magnetospheric plasma populations from ? showed significant local time asymmetry in the hot plasma population, with enhanced pressures in the dusk and midnight local time sectors compared to dawn and noon. These factors will therefore influence the magnetic and plasma configuration of the magnetosphere differently at different local times. It was shown by ? that variations in the hot plasma pressure, estimated using observations from ?, have a significant impact on the magnetospheric magnetic

field configuration. They found that a globally elevated hot plasma pressure causes a more disc-like magnetic field structure, due to the enhancement of the equatorial ring current, and that this also influences the magnetic mapping between the equatorial disc and the ionosphere. We have also previously discussed in this thesis how modelling results suggest that more expanded systems, with larger magnetopause radii, typically have a more disc-like magnetic field structure, due to overall force balance (e.g. ???). This is also seen in observational studies such as ?, who find that in the noon sector, Saturn’s magnetosphere only shows a significant divergence from a dipolar field structure for a magnetopause radius greater than $\sim 23 R_S$, but that the magnetodisc structure is consistently observed on the flanks and nightside, where the magnetopause radius is greater.

In this work we investigate the relative importance of the hot plasma pressure and magnetopause radius asymmetries in controlling magnetospheric structure at different local time sectors using a modelling approach, to complement observational studies. We use the University College London/Achilleos-Guio-Arridge (UCL/AGA) model, adapted to describe the typical, equilibrium conditions of Saturn’s magnetosphere at four different local time sectors; noon (09:00-15:00), dawn (03:00-09:00), dusk (15:00-21:00) and night (21:00-03:00). We use equatorial profiles of the hot plasma pressure from ? for the different local time sectors as boundary condition inputs to the magnetodisc model, and determine appropriate magnetopause radius values to use for each sector based on the magnetopause surface model of ?. Our method of constructing these models is described in Section ???. In Section ?? we present the results of these calculations, and highlight interesting comparisons in the magnetic field structure, azimuthal current density and magnetic mappings for the different local time sectors. Section ?? provides a brief summary of the main conclusions of this work.

2.2 Method

In this study we used a modified version of the UCL/AGA magnetic field and plasma model first set out in ? and described in Section 1.5. As a reminder, the model is axisymmetric about the planetary dipole/rotation axis, which are assumed to be parallel, and is constructed based on the assumption of force balance in the rotating plasma of the magnetosphere. The model assumes the magnetospheric plasma

Table 2.1: Coefficients of fourth order polynomial fits to the logarithm of each of the hot pressure profiles shown in Figure ??, as described in the main text.

Coefficient	Noon	Dawn	Dusk	Night
a_0	-5.47	-1.96	-1.36	-6.86
a_1	1.10	-0.149	-0.311	2.07
a_2	-0.114	0.0686	0.109	-0.258
a_3	0.00514	-0.00652	-0.0104	0.0137
a_4	-8.47×10^{-5}	1.83×10^{-4}	2.99×10^{-4}	-2.71×10^{-4}

comprises a cold population with pressure P_C , confined towards the rotational equatorial plane due to the centrifugal force exerted on it, and a hot population with associated plasma pressure P_H constant along magnetic field lines. The model calculates the magnetic field and plasma structure on closed magnetic field lines in 2-D space by iteratively solving a partial differential equation for the magnetic potential α . At each iteration, a linear combination of the previous and current solutions is calculated as input to the next iteration, in to slowly approach model convergence, as discussed in Section 1.5. In this study we found that, for nightside models with especially large disc radii, it was necessary to weight the previous solution up to nine times more heavily than the present solution in order to achieve convergence, corresponding to $\gamma = 0.1$ in equation 1.28.

The UCL/AGA model was originally used to represent typical dayside conditions at Saturn, and so we made various modifications described herein, which are necessary to appropriately represent different local time sectors.

2.2.1 Hot Plasma Parameterization for Different Local Time Sectors

An important boundary condition for this model is the global hot plasma pressure, as this strongly influences the resulting magnetic field structure, as discussed in Section ???. Recently, a comprehensive study using *Cassini* MIMI data (?) showed that the pressure of this hot plasma population not only varies over time and distance, but also varies significantly with local time, even when averaged over a large portion of the *Cassini* mission (July 2004 - December 2013). Therefore in this study, we used average equatorial profiles of hot plasma pressure between 5.5 and 15.5 R_S presented in ? for the different local time sectors, as boundary conditions for our models. Specifically, we fit the $1 R_S$ -width-binned data presented in ? using

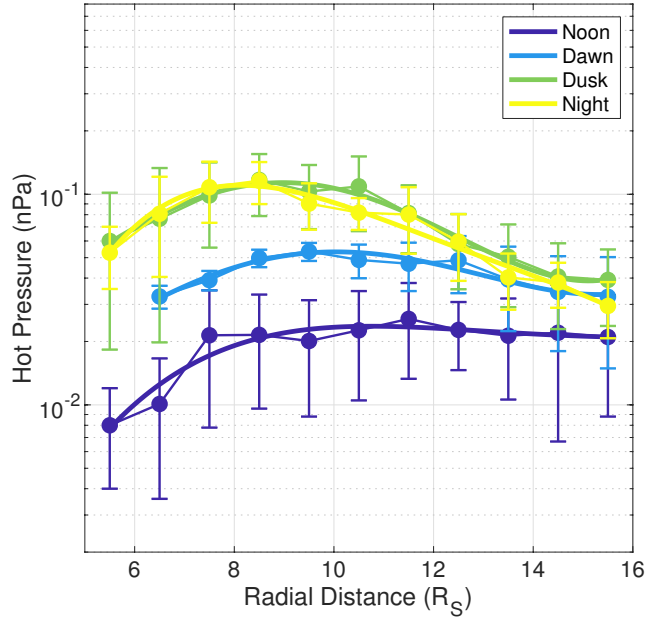


Figure 2.1: Equatorial radial profiles of hot plasma pressure for different local time sectors, as shown by the colour. Solid circles and error bars are means and standard errors for binned data from ?, and solid lines are 4th order polynomial fits to the logarithms of the data points, as described in the main text.

polynomial functions of the form

$$\log(P_H) = a_0 + a_1\rho + a_2\rho^2 + a_3\rho^3 + a_4\rho^4 \quad (2.1)$$

following the approach used in ?, with each point weighted by the inverse square of the provided standard error of the mean. The resulting coefficients for each sector are shown in Table ??, with pressure in units of nPa and radial distance in units of R_S . The polynomials are shown in Figure ??, as well as the corresponding observations from ?, with standard error of the mean of each bin shown by the error bars. This figure shows that the hot plasma pressure is significantly higher in the dusk and night sectors than the dawn and noon sectors. Here the dawn, noon, dusk and night sectors are defined by the magnetic local time intervals 03:00-09:00, 09:00-15:00, 15:00-21:00 and 21:00-03:00 respectively.

For values of ρ smaller than the applicable range of the polynomials ($5.5 R_S$) we assumed the hot plasma pressure falls linearly to zero with ρ , broadly in line with observations and with the approach of ?. For the dawn profile we used an inner boundary of $6.5 R_S$ due to lack of data in the innermost bin in the ? data,

Table 2.2: Configuration details for the two families of models used to represent different local time sectors, for compressed (high solar wind dynamic pressure) and expanded (low solar wind dynamic pressure) regimes. magnetodisc radius, shielding magnetic field value and an estimate for the solar wind dynamic pressure D_P are shown for each model.

Regime	LT Sector	Disc Radius (R_S)	Shield B_z (nT)	D_P estimate (nPa)
Compressed	Noon	21.0	-2.62	0.031
	Dawn	34.3	-0.97	0.026
	Dusk	33.2	-0.88	0.030
	Night	42.0	0.14	-
Expanded	Noon	27.0	-1.40	0.012
	Dawn	43.8	-0.47	0.015
	Dusk	42.3	-0.41	0.016
	Night	54.0	0.13	-

which can be seen in Figure ???. For values of ρ above the applicable range of the polynomials ($15.5 R_S$), we assumed a profile where the product of the hot plasma pressure and the local flux tube volume is constant with radial distance, following previous studies such as ???. In practice for the dawn and dusk models we used outer limits of $15.3 R_S$ and $15.1 R_S$ respectively, which are the locations of the local minima in the hot pressure polynomials, to ensure a smoother profile.

2.2.2 Magnetopause Radius for Different Local Time Sectors

The UCL/AGA magnetodisc model used in this work can also be parameterised by an effective disc radius R_D , the equatorial radial distance of the last closed field line in the model. As discussed in Section ?? and throughout this thesis, variations in this quantity also significantly impact the resulting magnetic field structure in the model. It was therefore important for this work that we chose appropriate values of the disc radius R_D for each of the local time sectors we were describing. To do this, we appealed to the study of ?, who improved the earlier Saturn magnetopause surface models of ??? by in particular including a small dawn-dusk asymmetry in magnetopause radius in the model. In ? the authors used observations of magnetopause crossings made throughout a large portion of the *Cassini* mission to constrain parameters for a ? type magnetopause model, introducing an extra parameter to describe the dawn-dusk asymmetry whilst maintaining a continuous surface at the magnetopause nose. They found that on average the magnetopause boundary extends farther from the planet on the dawn side than the dusk side, by ~7%.

In order to investigate how local time variation in magnetospheric structure varies with system size, we calculated two sets of models under different solar wind dynamic pressure conditions; a compressed regime with subsolar magnetopause radius fixed at $21 R_S$, and an expanded regime with subsolar magnetopause radius fixed at $27 R_S$, following the bimodal values observed in ? and ?. For the corresponding dawn and dusk disc radii, we calculated the magnetopause radius at the center of each local time sector (06:00 for dawn and 18:00 for dusk) using the best fit parameters given in ? and ?. We used a value of the nose plasma $\beta = 3$, which is the median value for the dataset quoted in ?, although for a fixed subsolar radius this choice of β had very little impact on the resulting flank radii. Thus we determined the appropriate disc radii R_D for noon, dawn and dusk local time sectors, for both high and low solar wind pressure conditions. The resulting values are shown in Table ???. In the absence of an accurate magnetopause model for the nightside of Saturn's magnetosphere, we used a disc radius of twice the subsolar magnetopause radius to represent an approximate nightside local time sector structure.

The solar wind dynamic pressure corresponding to a given equilibrium magnetodisc model can be estimated by assuming pressure balance across the boundary at the equator, as in Chapters ?? and ???. Specifically we can assume

$$\frac{B_{MS}^2}{2\mu_0} + P_{MS} = \left[k \cos^2(\psi) + \frac{k_B T_{SW}}{1.16 m_p u_{SW}^2} \sin^2(\psi) \right] D_P \quad (1.24 \text{ revisited})$$

where terms on the left hand side represent the magnetospheric magnetic and plasma pressures just inside the magnetopause boundary, and the terms on the right represent the component of solar wind dynamic pressure incident on the magnetopause surface, and a smaller component associated with the solar wind's thermal pressure. As explained in Section ??, $k = 0.881$ is a factor to account for the diversion of flow around the magnetosphere obstacle (see ?), $k_B T_{SW} = 100 \text{ eV}$ and $u_{SW} = 460 \text{ km s}^{-1}$ are the temperature and speed of the solar wind from ?, and ψ is the angle between the incident solar wind and the magnetopause surface normal. We used values for B_{MS} and $P_{MS} = P_H + P_C$ extracted just inside the magnetopause boundary of each model, and obtained ψ from the ? magnetopause surface model at the appropriate local time sector. The resulting estimates of D_P are shown in Table ???. This approach is not appropriate for the far night-side tail, where a concept of ψ is not di-

rectly applicable, and so we do not attempt to estimate D_P for those sector models. While the values of D_P do not exactly agree for all compressed or all expanded models, we can see that the two regimes provide significantly different, self-consistent estimates. The mean D_P estimates are 0.029 ± 0.003 nPa and 0.015 ± 0.002 nPa for the compressed and expanded regimes respectively, such that they broadly correspond systems under different solar wind conditions, whilst representing average internal conditions.

2.2.3 Magnetodisc Model Adaptations

Finally, we made minor adaptations to the magnetodisc model construction in order to be more appropriate for different local time sectors. As discussed elsewhere in this thesis, in ? the authors include a small, uniform, southward-directed ‘shielding field’ to the total magnetic field at every iteration, to approximately account for the magnetic field associated with the magnetopause and magnetotail current sheets. The magnitude of this field was chosen by calculating dayside equatorial averages of the empirical field models of ? and ?, and it varied with model magnetodisc radius R_D (see ?, Figure 6). For this study, we calculated local time sector averages of these field models, to account for the increased significance of the tail current field compared to the magnetopause current field for nightside local time sectors in particular. We also enhanced the field associated with the magnetopause current beyond a dipole approximation by a factor $(1 + k_{MD})$, where k_{MD} is the ratio of the ring current and planetary dipole magnetic moments, as in the study in Chapter ???. As described in Section ??, to estimate the appropriate k_{MD} for each model we employed an extrapolation of the empirical linear fit from ?, although here we used our values of R_D rather than the subsolar magnetopause radius to estimate k_{MD} as we found that this in particular improved convergence in our models. The resulting values for the shielding magnetic field B_z for each model are shown in Table ???. It can be seen that, as expected, the total shielding field decreases and becomes northward directed for the nightside models due to the increased influence of the more northward field associated with the distant tail currents, compared to the more southward field associated with magnetopause currents. While the use of these shielding field values does not significantly affect the global magnetic field structure of the resulting models, we find it does improve the tendency for our models to

achieve convergence.

We also updated the representation of the cold equatorial ion temperatures used as a boundary condition in the magnetodisc model, using a recent comprehensive survey of equatorial *Cassini* CAPS observations from ?. We fit the equatorial profiles of parallel and perpendicular temperatures for hydrogen and water group ions between 5.5 and $30 R_S$ presented in ? with fourth order polynomials, with points weighted by the inverse square of the error (assumed to be half the interquartile range of each bin). We then derived a single equatorial plasma temperature profile for the magnetodisc model as in ?, who used the same approach but with earlier more restricted data sets from ? and ?. The best fit polynomials for each ion species and temperature moment are given in the Appendix, ??, along with a comparison of the original profiles from ?. We found that this modification did not significantly affect the overall resulting magnetic field profile of the magnetodisc model, in general causing only a slight increase in magnetic field strength in the inner magnetosphere, and slight decrease in the outer magnetosphere, with a maximum difference under 1 nT . However this modification did improve model estimates of the cold plasma pressure, reducing the values in the outer magnetosphere such that they showed better agreement with recent observations from ? (also based on CAPS data). This modification represents better radial coverage and global constraint of the cold plasma temperature than in previous studies.

2.3 Results and Discussion

2.3.1 Magnetic Field Structure

The equatorial magnetic field profiles from the resulting magnetodisc models for each local time sector are shown in Figure ???. For comparison, a representative profile for the internal planetary dipole magnetic field is shown by the grey dashed line on each plot.

For the dayside (noon) models, we can see that the magnetic field is approximately dipolar in the inner ($\lesssim 10 R_S$) magnetosphere, and falls more slowly with radial distance than a dipole in the middle ($10 \lesssim \rho \lesssim 15 R_S$) and outer magnetosphere. This behaviour broadly corresponds to a more ‘disc-like’ magnetic field structure compared to a dipole, and appears for a more significant range in radial distance for the expanded noon model. Similar behaviour has been found in

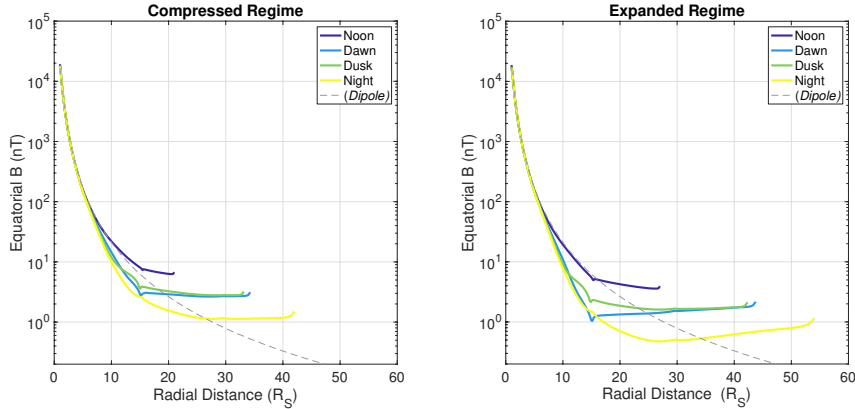


Figure 2.2: Equatorial profiles of total magnetic field strength B with radial distance for each local time sector as shown by the colour, for both the compressed (a) and expanded (b) regimes. On each plot a profile for a dipole magnetic field is shown in dashed grey for comparison.

observational studies of Saturn’s magnetosphere. For example ? showed that the dayside magnetospheric magnetic field was approximately dipolar when the system was compressed, but more disc-like when expanded, particularly beyond a sub-solar magnetopause radius of $\sim 23 R_S$. Results of ring current modelling from ? found a similar result.

For the larger dawn, dusk, and night sector models, the model magnetic field strengths are lower than the corresponding dipole field in the inner magnetosphere, and greater in the outer magnetosphere. This too is in line with *in situ* observations of Saturn’s magnetosphere, such as ?, who analysed equatorial current sheet crossings using *Cassini* MAG data, in order to demonstrate how the equatorial magnetic field varies with radial distance in different local time sectors. There is also a small dawn-dusk asymmetry in the magnetic field strengths in our model, with the dusk sector profile persistently higher than the dawn. This is likely a consequence of force balance, with the slightly higher hot plasma pressure in the dusk sector requiring a greater magnetic curvature force to balance it. This is interesting to note, as such a small asymmetry in field strength would be unlikely to reveal itself in observational studies of Saturn’s magnetosphere, especially due to the relatively poor sampling of the dawn sector equatorial magnetosphere by the *Cassini* spacecraft over its mission.

Looking at the day-night asymmetry in more detail, in Figure ?? we show the magnetic field structure for our noon and nightside magnetodisc models, for the compressed (top panel) and expanded (bottom panel) regimes. For comparison, we

include in red an empirical magnetic field model from a recent study by ?. In that study the author binned magnetic field observations from the entire *Cassini* mission into two local time sectors, dayside and nightside, and fit these using polynomial functions of latitude in order to derive a simple analytical model of Saturn's meridional magnetic field lines. ? accounted for seasonal warping of the current sheet via a coordinate transformation, although the polynomial functions still include terms that enable asymmetry across the rotational equator. However unlike in this study, the ? did not account for a change in external solar wind conditions, and so we have reproduced the same model output from ? in the top and bottom panels. We can see that the overall magnetic field structures in our models are similar to those of the ? model, in particular the expanded $27 R_S$ dayside model, and the compressed $42 R_S$ nightside model. In addition, the somewhat blunt, 'blockish' shape of the dayside field lines in the ? model are somewhat accentuated by the polynomial representation the author used, with the original traces of field lines presented showing a structure even more similar to our models presented here. Only our expanded nightside model shows a magnetic field structure that is significantly more disc-like than the ? analytical model, suggesting that perhaps a magnetodisc radius of $54 R_S$ is somewhat too extreme to accurately characterise the typical midnight magnetosphere. However in general the agreement is very good, suggesting our models can characterise the overall structure of the magnetospheric magnetic field at different local times, provided the disc radius is chosen appropriately. Also, we should note that here we are comparing specifically our noon (LT 03:00-09:00) and night (LT 21:00-03:00) sector models, with the ? models which correspond to wider, 12 hour local time regions. Therefore to more accurately represent (for example) the entire dayside for a more direct comparison, we would need to consider some combination of our noon, dawn and dusk sector model outputs.

In order to investigate more just how 'disc-like' the magnetic field is in each local time sector, we use a visualisation technique employed in ?, where for each model we bound regions of the magnetosphere where the local magnetic field direction lies within 30° of the equatorial plane, such that the field lines are approximately parallel to the equatorial plane. The results are shown in Figure ??, and the reproduction of the most lower latitude of the bounding lines are shown in Figure ???. The magnetic

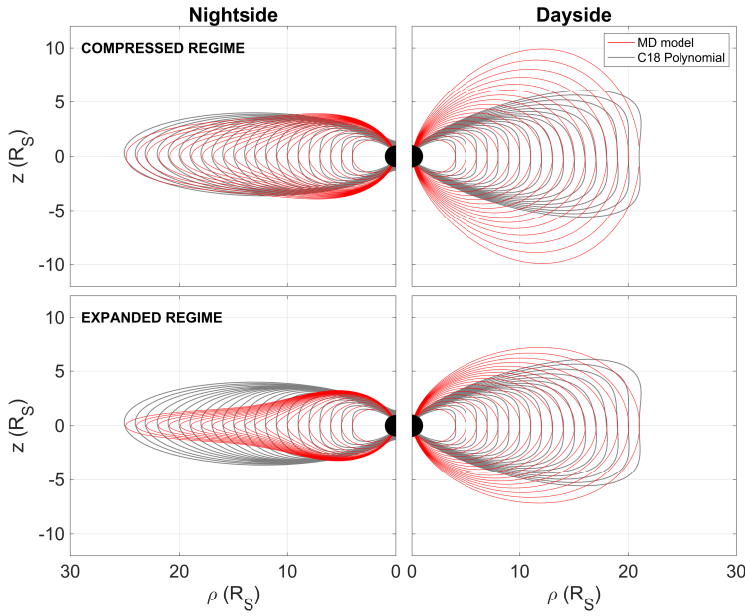


Figure 2.3: A comparison of model magnetic field lines from ? and this study. In grey are shown polynomial fits to binned *Cassini* magnetometer meridional magnetic field observations from ? (top and bottom panels an exact reproduction). In red are shown magnetic field lines from the noon and nightside models presented in this study, for the compressed (top panel) and expanded (bottom panel) regimes, for L shells to match those of the ? study.

field structure for each model is also shown in black, to further illustrate how this method characterises the ‘discy-ness’ of the magnetic field structures. These figures show that, as expected, the larger magnetodisc models have significantly more disc-like magnetic field structures in the middle magnetosphere, than the smaller, more dipolar models. As discussed in the introduction, this was observed in previous studies such as ??? and is a result of how the overall force-balance within the magnetosphere changes with system size, in terms of the dominant magnetic and plasma related forces.

In addition, from Figure ?? in particular, it can be seen that, for the compressed regime, the dusk sector has a slightly thinner and more disc-like magnetodisc structure in the middle magnetosphere than the dawn sector, as shown by the bounding lines being more equatorward for the dusk model (shown in green). This effect is likely due to the local enhancement of the ring current in the dusk sector due to the increased hot plasma pressure, which causes a more extreme perturbation from a dipolar magnetic field. This was also discussed in the introduction, and observed in ???. Note that this ‘thinning’ of the disc is not the same as thinning of the *plasma* sheet, which is made up of both hot and cold plasma populations. While the *current*

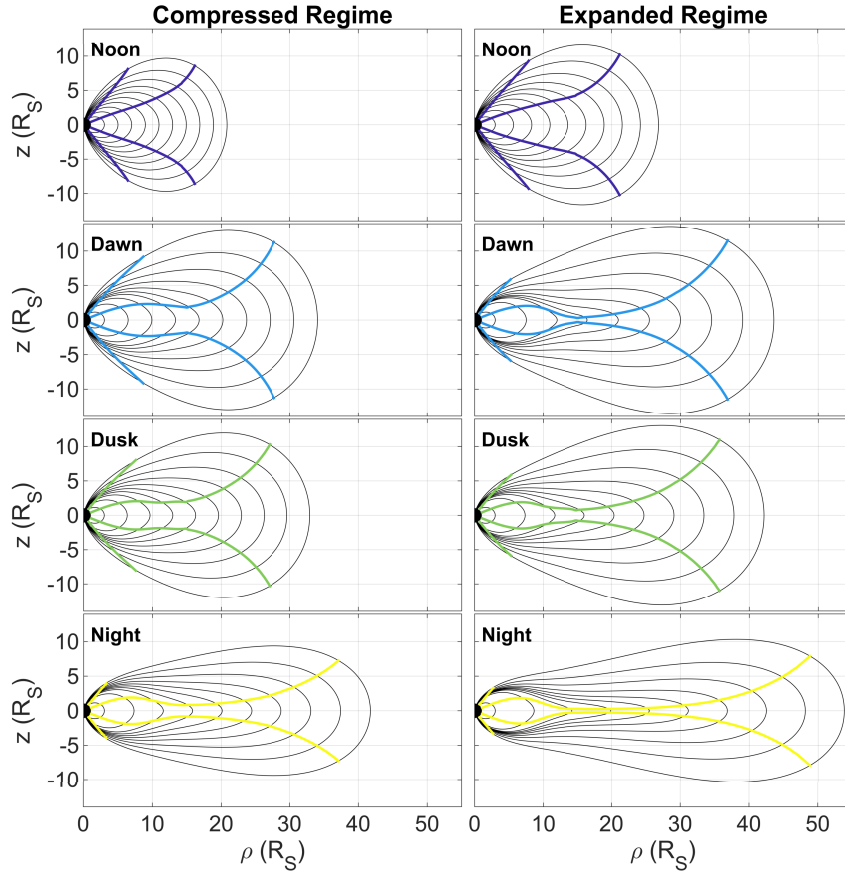


Figure 2.4: The magnetic field structure for each magnetodisc model for the compressed (left column) and expanded (right column) regimes, shown by the solid black lines. Superposed in colour for each model are pairs of lines in each hemisphere which bound regions where the local magnetic field direction lies within 30° of the equatorial plane.

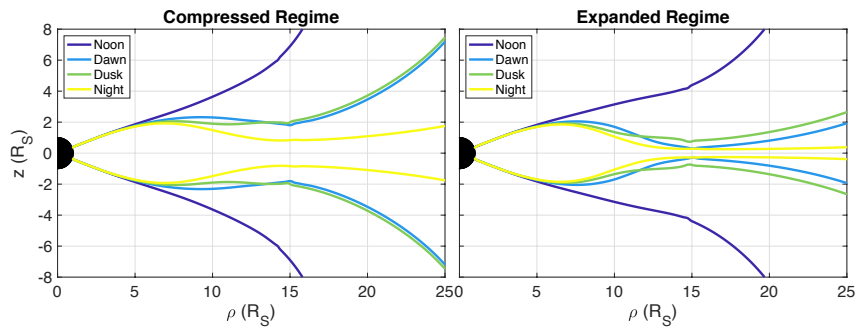


Figure 2.5: Reproduction of the more equatorward coloured lines from Figure ??, for each local time sector model, for compressed (left) and expanded (right) regimes. These represent the low latitude boundaries of regions where the local magnetic field direction lies within 30° of the equatorial plane.

sheet and associated *cold* plasma sheet thins, the hot plasma is actually more populous for the thinner, dusk model, and the associated hot plasma pressure is constant along magnetic field lines. As described in ?? the current sheet, a predominantly magnetic structure, has been observed to be thinner than the plasma sheet it is embedded in, and the plasma sheet itself can have different thicknesses in different particle energies and species.

For the expanded regime, it can be seen in Figure ?? that the opposite relationship is true, and that in the middle and outer magnetosphere, the dawn sector magnetic field has a thinner and more disc-like structure (shown in blue). This is likely due to the increased influence of the dawn-dusk asymmetry in effective magnetodisc radius for the expanded regime, as a larger magnetopause radius also promotes a more disc-like structure. For the expanded regime, the dawn magnetopause is $1.5 R_S$ greater than the dusk, compared to $1.1 R_S$ for the compressed regime. It is interesting that this transition in dominant behaviour occurs across this compressed-expanded regime threshold. These results suggest that the asymmetries in magnetopause radius and hot plasma content have comparable influence on the global magnetic field structure in those local time sectors. In addition, the expanded system models may be more strongly influenced by the assumption we made that the product of flux tube volume and hot plasma pressure is constant beyond $15.5 R_S$, as described in Section ??, as this region is by definition more extended for the expanded system models, where R_D is greater. We hope to relax this assumption with an updated parameterization of the hot plasma pressure beyond $15.5 R_S$ in a future study.

In the aforementioned study by ?, the authors find significantly more incidences of ‘critically thin’ equatorial current sheet encounters in the dusk sector than the dawn sector, even when accounting for the sampling bias of *Cassini* (which spent more time in the dusk sector). This is therefore more in line with our picture of the compressed regime, with a thinner current sheet on the dusk side due to the influence of the increased hot plasma pressure. In contrast, in a study from ?, based on MHD simulations of Saturn’s magnetosphere from ?, they find the opposite behaviour, with a significantly thinner current sheet and more radially stretched magnetic field lines in the dawn sector, which is also observed at Jupiter (e.g. ?). This may be

understood, as that the simulations of ? do not include a suprothermal plasma population, and so the effect of the enhanced hot plasma population on the dusk side is not captured in their study. In addition, it was suggested by ? that this absence of suprothermal plasma in the ? models may cause their models to slightly overestimate the dawn-dusk asymmetry in magnetopause radius, which predict a mean asymmetry of $2.6 R_S$, compared to $1.6 R_S$ for the ? empirical model. Therefore the results of ? may be more strongly influenced by this asymmetry in magnetopause radius, which, as discussed, provides a thinner and more disc-like current sheet in the dawn sector. However, their MHD models do account for plasma acceleration, and azimuthal asymmetry in the magnetic field, which the force-balance models presented in this study do not. Therefore some dawn-dusk asymmetry in these factors may also influence current sheet thickness in ways that our model cannot capture.

2.3.2 Ionospheric Field Line Mapping and Azimuthal Current Density

We discussed in Section ?? varying hot plasma content and magnetopause radius can both affect the mapping of magnetic field lines from the equator to the ionosphere, due to a reconfiguration of the magnetospheric magnetic field structure. It is therefore important to consider how this ionospheric mapping varies for different local time sectors.

The inner boundary of our magnetodisc model is located at a radial locus of $1 R_S$ where $R_S = 60\,268 \text{ km}$, specifically the *equatorial* radius of Saturn at 1 bar atmosphere level. This is greater than the *polar* radius at 1 bar, as Saturn is oblate. Our model therefore does not directly calculate the magnetic field in the polar ionospheric regions, as these regions are closer to the planet than the inner boundary of our model. Also, our model assumes a centred dipole planetary magnetic field. Therefore we need to account for the oblate spheroid shape of the planet, the altitude of the ionosphere, and effective offset of the planetary dipole in our ionospheric mapping calculations. We do this by calculating the magnetic potential α (see discussion in Section ??) for a dipole magnetic field with origin offset northwards by $z_{\text{off}} = 0.0466 R_S$ (?), along a surface 1100 km altitude above an oblate spheroid with equatorial radius 60 268 km and polar radius 54 364 km (?). The ionospheric altitude

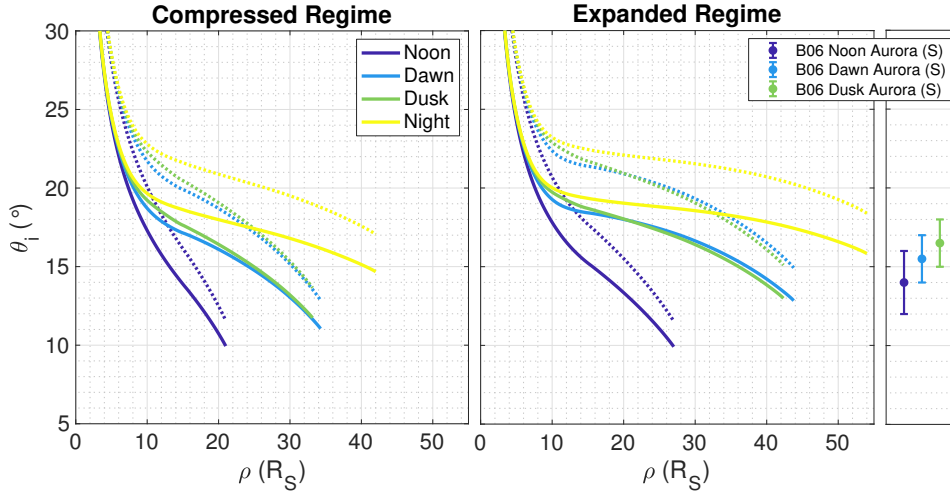


Figure 2.6: Equatorial profiles showing the mapping of magnetic field lines from the equatorial plane to the northern (solid lines) and southern (dotted lines) ionospheres, with local time sector shown by the colour. Ionospheric colatitude θ_i is measured relative to the northern pole for northern hemisphere values, and the southern pole for southern hemisphere values. Also shown by the solid circles with error bars are median locations and widths of the main auroral oval in the southern hemisphere for different local time sectors as shown by the colour, from a statistical study by ?. Model values shown here are provided in tables in the Supporting Information to ?, submitted.

of 1100 km was chosen following studies from ?? and others. As the magnetic potential α is constant along a given magnetic field line by definition, we can then map equatorial values of α to the oblate ionospheric surface in order to estimate the realistic colatitude at which the magnetic field lines would pierce the northern and southern polar ionospheres.

The resulting values are shown in Figure ??, with northern hemisphere values shown by solid lines and southern hemisphere counterparts shown by dotted lines. All values shown in Figure ?? are also provided in tables in the Supporting Information to ?, submitted. Also shown by the coloured solid circles with error bars are the average locations and widths of the main auroral oval for noon, dawn and dusk local time sectors respectively, estimated from a statistical study of multiple Hubble Space Telescope (HST) observations of the UV aurora in the southern hemisphere from ?. As these observations were of the southern hemisphere only, they should be compared with the dotted lines of the model outputs.

It can clearly be seen that there is significant variation in ionospheric mapping of field lines for different local time sectors. In particular, the locations of the open-closed field line boundary (OCFLB), shown by the colatitude of the most radially

distant point for each profile, vary greatly between sectors. We can see that the OCFLB maps to more polar regions in the noon sector, with $\sim 10^\circ(11.5^\circ)$ for the northern (southern) hemisphere, than for the night sector, with $\sim 15.5^\circ(17.5^\circ)$ for the northern (southern) hemisphere. This behaviour is qualitatively in agreement with the results of ?, who find corresponding values of $\sim 13^\circ(16^\circ)$ for the dayside, and $\sim 16^\circ(18^\circ)$ for the nightside, using a data-based magnetic field model. Our noon sector values are somewhat lower than the dayside values of ?; however, if we were to consider some combination of our noon, dawn and dusk values to represent the entire dayside hemisphere, for a more appropriate comparison, they would likely be in better agreement. This is because the values for dawn and dusk are both higher than the noon value alone.

In addition, for the compressed regime in particular, we find a slight dawn-dusk asymmetry in the location of the OCFLB, with the dusk location around 1° equatorward of the dawn location. It can be seen on close inspection of Figure ?? that this asymmetry is mainly due to the small asymmetry in magnetopause radius in these models, rather than the influence of the hot plasma pressure profiles on the magnetic field structure. This is evident as the two profiles are broadly coincident in the outer magnetosphere until the dusk model terminates at $\rho = 33.2 R_S$, in comparison to dawn's $34.3 R_S$ (see Table ??). It is interesting to note that this relationship is qualitatively similar to that observed by ?, who found that on average the main auroral oval in the dusk sector was located $\sim 1^\circ$ equatorward of the aurora in the dawn sector, in the southern hemisphere. Furthermore, the dawn aurora was observed to be $\sim 1.5^\circ$ equatorward of the noon auroral location in ?. This is approximately the same as the difference in the OCFLB we observe between our noon and dawn models for the compressed regime, southern hemisphere values, as shown in the first panel of Figure ?? (although the difference is significantly higher for the expanded regime). Such a comparison supports the hypothesis from this and other studies, that the main auroral oval may map to regions in the outer equatorial magnetosphere, within a few R_S of the OCFLB. In addition, a later study by ? of Saturn's infrared aurora found that the nightside main oval was persistently $\sim 2^\circ$ equatorward of the dayside, in line with the aforementioned day-night asymmetry we observe in our OCFLB. It is interesting to note that this agreement is achieved

despite the shielding field associated with the UCL/AGA model, discussed in Section ??, being a less accurate approximation in the higher latitude regions, beyond around 50° latitude (?).

Now comparing the results for the compressed and expanded regimes, we see that the differences between the profiles are not as extreme as the differences between local time sectors. This suggests that variations in external solar wind conditions do not have a significant impact on the magnetic mapping between ionosphere and the equatorial disc. In particular for the noon sector, the profiles for the compressed and expanded regimes are very similar, with near coincident locations of the OCFLB, and similar regions of the equatorial magnetosphere mapping to similar values of θ_i in each case. For example, the equatorial radial distance corresponding to the outer one-third of the noon sector magnetosphere for each regime, maps to roughly the same θ_i for each case, $\sim 14^\circ$ in the north, and $\sim 16.5^\circ$ in the south. A similar result was found in ?, who used an adapted “CAN” type (??) ring current model from ? to investigate how ionospheric mapping varied with system size in the noon sector magnetosphere. They found only a very modest variation with system size, for a noon magnetopause radius range of $16 - 26 R_S$, comparable to the range in this work. ? then used the results of this modelling, in combination with HST observations of the UV aurora and *Cassini* data, to show that the noon aurora are indeed likely to lie near the boundary between open and closed magnetic field lines. These authors go on to suggest that the quasi-continuous main auroral oval corresponds to the OCFLB at other local time sectors, in line with our interpretation here. Combining results for all local time sectors and compressed/expanded regimes, we find a mean location of the OCFLB equal to 12.4° in the north and 14.4° in the south. This is comparable to recent results from a *Cassini* multi-instrument study from ?, who find corresponding values of 13.3° in the north and 15.6° . In that study, the majority of observations are from the post-midnight sector where we expect the OCFLB to be more equatorward, which may explain why their average values are a little higher than ours.

When interpreting ionospheric-equatorial magnetic mappings, it is also pertinent to consider how the total current density varies with radial distance in the equatorial magnetosphere. Predictions for total azimuthal current density at the

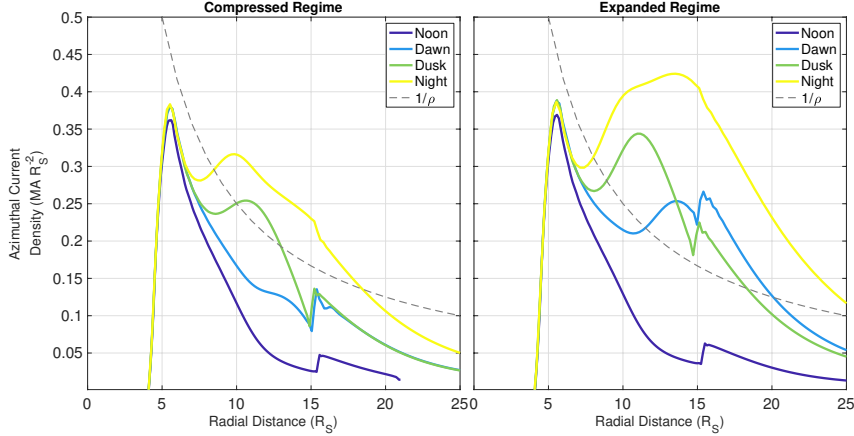


Figure 2.7: Profiles of equatorial azimuthal current density with radial distance, for each local time sector model as shown by the colour, for compressed (left) and expanded (right) regimes. The grey dashed line shows a representative profile with current density inversely proportional to radial distance, as for a ?? style ring current model.

equator for each local time sector model, for compressed and expanded regimes, are shown in Figure ???. (Note that as the magnetodisc model is azimuthally axisymmetric, and hence used here to represent individual local time sectors separately, radial currents are not directly predicted.) Superimposed on each plot is a representative profile with azimuthal current density inversely proportional to cylindrical radial distance ρ , as is the case for CAN type ring current model constructions from ??.

We can clearly see significant dawn-dusk and noon-night asymmetry in the current density profiles, with higher magnitudes for the dusk and night sector models, for both the compressed and expanded regimes. This is due to the similar relationship between the different input equatorial hot plasma pressure profiles for each local time sector, shown in Figure ??, enhancing the component of the ring current associated with the hot plasma pressure gradient. In addition, the underlying magnetic field structure, and the centrifugal force on the cold plasma, both influence the current density profile via equation (??). This helps explain the significant difference in all profiles between the compressed and expanded regimes, with larger models having in general higher magnitude predicted azimuthal currents, due to lower magnetic field strengths at the equator as shown in Figure ???. The nightside models in particular have much higher predicted current densities than all other sector models for this reason. Similar results were also shown in a study by ?; in that study, the authors presented results of MHD simulations of Saturn's magnetosphere and

ionosphere, and found that the predicted azimuthal current density had a persistent local time asymmetry, being higher by a factor of $\sim 2\text{--}3$ on the nightside than at other local times. In addition, it is interesting to note that for the expanded regime, the region $\rho \approx 13R_S$ where the current density at dawn surpasses the current density at dusk, is almost coincident with the region where the dawn magnetic field structure becomes more disc-like than dusk, as shown in Figure ???. This further illustrates the relationship between ring current activity and magnetodisc magnetic field structure.

From Figure ?? we can also see that for all local time sectors, beyond the local maximum region, the equatorial current density falls more quickly than the $1/\rho$ decrease predicted by a CAN type ring current model. Similar behaviour was also found in the observational study from ?, who used *Cassini* MAG, MIMI and CAPS observations to make estimates of equatorial azimuthal density profiles, and found local maxima for each sector profile in the radial range $\sim 7 - 13 R_S$, followed by a fast decay with radial distance. This suggests that the more complex ring current structure enabled by the modified UCL/AGA model used in this study may be more appropriate at characterizing the true structure of Saturn’s equatorial current sheet than a CAN type model. However both types of model give similar predictions for the magnetic field away from the edges of the CAN disc, as discussed in ?.

2.4 Summary and Conclusions

In this study we have used the 2-D, force-balance UCL/AGA model from ? to describe the typical, equilibrium conditions of Saturn’s magnetosphere at four different local time sectors. We have used equatorial profiles of hot plasma pressure at different local times from ?, and a magnetopause surface model from ?, to investigate how global hot plasma content and system size influence the magnetospheric structure at different local times.

We have found that, as expected, there is significant day-night asymmetry in the magnetic field structure of the magnetosphere, and that this is mainly due to the large asymmetry in magnetopause radius between day and night. We also find a small dawn-dusk asymmetry in the magnetic field structure, with both the hot plasma content and magnetopause radius having comparable influence. For the compressed regime, where the magnetosphere is under high solar wind dynamic

pressure conditions, we find that the dusk sector magnetic field is more disc-like due to the influence of the increased hot plasma pressure in that sector. Meanwhile for the expanded regime we find the opposite is true, and that the dawn magnetic field is more disc-like, due to the larger magnetopause radius at dawn for this regime. Importantly, we also find significant differences in how equatorial magnetic field lines map to the polar ionosphere for the different local time sector models, with field lines from the outer magnetosphere mapping to far more equatorward regions of the ionosphere on the nightside than the dayside. This result is useful in particular when interpreting auroral observations at Saturn’s ionosphere and attempting to ascertain their origins in the magnetosphere. These results may also be useful for future studies looking at local time variations in other magnetospheric properties, such as current sheet thickness.

The simplicity of the modelling approach used in this work means that many magnetospheric properties can be easily compared between different local time sectors. However a consequence of this is that any dynamical behaviour, such as reconnection events or plasmoids, cannot be directly captured. In addition, due to the assumed axisymmetry of each model, we cannot investigate the influence of any observed local time asymmetry in azimuthal phenomena. For example, a non-negligible dawn-dusk asymmetry in the azimuthal ‘bend-back’ of magnetic field lines in the direction opposite to planetary rotation has been observed, with more substantial bend-back in the dawn sector than the dusk sector (e.g. ?). This may affect our assumptions of how magnetospheric plasma properties vary with radial distance, such as the angular velocity, which in turn influences our estimates of centrifugal force. In ?, the authors offer a formulation for how the force balance assumption of equation (??) could be modified to account for a local time variation in radial outflow of plasma. While a preliminary investigation suggests this approach would not have a significant impact on our results, it would be worthwhile to investigate this further in a future study.

In summary, this study shows that there is significant local time variation in the magnetic field structure of Saturn’s magnetosphere. The equatorial current sheet thickness, current density and magnetic mapping to the ionosphere all vary depending on both local time and external solar wind pressure conditions, due to

force balance within the magnetosphere in this study. Our results are useful for potential future studies looking to interpret a range of phenomena at Saturn, from reconnection events and plasmoids to auroral oval modulations.

Chapter 3

Conclusions and Directions for Future Work

3.1 Impact of System Size on Large-Scale Structure and Dynamics

In this thesis we have studied in detail how the large-scale structure and dynamics of Saturn’s magnetosphere varies with system size. In Chapter ??, we used the UCL/AGA model to investigate specifically how the compressibility of the magnetosphere varied with system size, and in Chapter ?? we looked at how the large-scale structure varied at different system sizes across a range of local times. The size of the magnetosphere is in turn influenced by the upstream solar wind conditions; in Chapter 1 we discussed how the magnetopause location is determined to the first order by pressure balance between the solar wind dynamic pressure D_P and the internal magnetospheric plasma and magnetic pressures, and how D_P varies with both the density and speed of the solar wind plasma.

Our modelling results presented in Chapters ?? and ?? suggest that the large-scale structure of Saturn’s magnetosphere is more disc-like when the system is expanded, beyond a sub-solar magnetopause radius of $\sim 25 R_S$. This *magnetodisc* configuration is associated with more radially stretched field lines in the middle magnetosphere near the equatorial plane around a thin equatorial current sheet, and a total magnetic field strength that falls more slowly with radial distance than a dipole magnetic field. If the system is compressed by increasing solar wind dynamic pressure, the magnetospheric magnetic field then reconfigures into a more dipolar structure, with a correspondingly thicker equatorial current sheet.

Similar results were found in the empirical study by ?, based on *Cassini* magnetic field observations. In that study, the authors surveyed *Cassini* magnetometer data for current-sheet-like fields, and examined the distribution of observations that fit a certain set of criteria corresponding to a distorted, stretched magnetic field configuration. They found that a significant magnetodisc structure only formed on the dayside when the system was expanded with a sub-solar radius beyond $\sim 23R_S$, and that for smaller systems, a magnetodisc only formed on the nightside and flanks. They suggested that this is due to the near-coincidence of the expected inner boundary of the magnetodisc based on stress balance, and the nominal subsolar magnetopause, meaning the disc is prevented from forming under compressed conditions. This is in agreement with the results of the study by ?, based on models of the ring current from ?, which found that the magnetic moment of the ring current increases as the system expands, causing a more extreme distortion of the magnetospheric magnetic field in such conditions. This behaviour was also suggested in the original UCL/AGA model study based on a comparison of two models calculated at different sizes ?.

In a steady-state system, we can consider this reconfiguration from a dipolar to a more disc-like structure as determined by force balance in the rotating plasma of the magnetosphere, between the centrifugal force, plasma pressure gradient force and ' $\mathbf{J} \times \mathbf{B}$ ' Lorentz body force. In Section 1.1.2 we showed how this Lorentz body force is equivalent to the sum of a magnetic pressure gradient force, and a magnetic tension force. Near the equatorial plane, the main force acting radially inwards is the component of the magnetic tension force perpendicular to the magnetic field, which is proportional to B^2/r_c (where r_c is the magnetic field line radius of curvature). As the system expands, the magnetic field strength in the outer magnetosphere falls, and so in order for the magnetic tension force to balance the centrifugal and plasma pressure gradient forces acting radially outwards, the radius of curvature of the magnetic field lines must decrease. This corresponds to a more disc-like magnetic field structure, supported by a thin sheet of azimuthal current that extends far into the outer magnetosphere.

This becomes particularly important when investigating how Saturn's magnetospheric structure varies across local time, as the nominal magnetodisc is signifi-

cantly larger on the nightside and flanks of the magnetosphere than on the dayside. In addition, recent results from ? suggest a small dawn-dusk asymmetry in the typical magnetodisc size. In Chapter ??, we presented results of a modelling study which suggested that this variation in system size did indeed influence the magnetic field structure at different local times, which in turn influences magnetic mapping between the equatorial disc and the ionosphere. We found that in particular the open-closed field line boundary mapped to more equatorial regions of the ionosphere for expanded systems than compressed systems, which has impacts for interpreting ionospheric phenomena such as aurora, as discussed in that chapter.

In Chapter ?? we used a family of UCL/AGA models calculated at different sizes in the range $45-55 R_S$, and organised with Saturnian ‘longitude’, to simulate a periodic thickening and thinning of Saturn’s magnetospheric current sheet in response to the dual rotating magnetic perturbations discussed in Section 1.4.1. We found that, when combined with a geometrical model of a tilted and rippled current sheet surface, this model characterised well the observed periodic perturbations in the magnetic field measured by *Cassini* in Saturn’s outer magnetosphere. In particular we found that the meridional component of the magnetic field was much better characterised when this perturbation in the magnetodisc size was included. This suggests that our approach of using an oscillating boundary location with a $10 R_S$ range appropriately simulates the corresponding change in magnetodisc structure and current sheet thickness, although with caveats as discussed in Chapter ???. Evidence for periodic perturbations in the magnetopause boundary was found in the empirical study by ?, and also the MHD modelling study ?.

This reconfiguration of the magnetic field under compressed conditions also influences the compressibility of the dayside magnetosphere in response to changing solar wind dynamic pressure. In Chapter ?? we presented results of a modelling study which suggested that the magnetosphere becomes more easily compressible as it expands, due to the more significant magnetodisc structure under such conditions. As previously mentioned, a more significant magnetodisc structure has a magnetic field profile with strength varying more slowly with radial distance than a dipole, due to the magnetic field associated with the azimuthal ring current. This affects the pressure balance between the magnetic pressure and the solar wind dynamic

pressure at the magnetopause boundary, and thus the compressibility, making the magnetosphere size more sensitive to a given change in solar wind dynamic pressure. A similar result was found in the aforementioned ring-current modelling study of ?, due to similar arguments of the magnetodisc structure becoming more significant for an expanded system.

We showed in Chapter ?? that this is contrast to the Jupiter system, which seems to show a magnetospheric compressibility behaviour that is approximately constant across system size. We suggested that this was because unlike at Saturn, Jupiter's magnetosphere has a consistent magnetodisc magnetic field structure across the full range of observed system sizes, even when extremely compressed under high solar wind pressure conditions. Therefore the magnetic field pressure, which dominantly controlled the compressibility in our UCL/AGA modelling results, varies self-similarly with radial distance for the different system sizes. This more stable magnetodisc structure at Jupiter is due to a range of factors, first discussed in Section 1.3.2. Jupiter has a more significant internal source of plasma than Saturn, originating from the volcanic moon Io, and also rotates more rapidly, with a 9.9 h period compared to Saturn's \sim 10.6 h. In addition, the overall size-scale of Jupiter's magnetosphere is greater, with typical magnetopause stand-off distance of \sim 75 R_J, due to the larger internal planetary magnetic field at Jupiter (details in Table ??), and this internal plasma population. Therefore the centrifugal force exerted radially outwards on the magnetospheric plasma is greater at Jupiter than at Saturn, causing a more significant distortion of the magnetic field into a magnetodisc structure, supported by an intense ring current (e.g. ?). As a consequence, Jupiter's magnetosphere has a more stable magnetodisc structure particularly on the dayside when compared to Saturn, despite being significantly closer to the Sun and therefore experiencing higher average solar wind dynamic pressures. In contrast, if Saturn were located at Jupiter's position in the solar system, it would show a uniform compressibility behaviour across system size, specifically corresponding to its compressed, more rigid regime. Therefore the impact of varying system size on the large-scale structure and dynamics of each planetary magnetosphere varies depending on both internal and external influences.

3.2 Impact of Hot Plasma Population on Large-Scale Structure and Dynamics

In this thesis we have also investigated in detail how the large-scale structure and dynamics of Saturn's magnetosphere are influenced by the presence of an internal, global hot plasma population. It is pertinent to study the impact of this population in particular as observational studies have shown that this population varies significantly over short timescales (?) and in local time (?), suggesting that its influence may vary across these domains. This is in contrast to the more stable population of cold plasma originating from Saturn's icy moon Enceladus, which is confined towards the equatorial plane due to the centrifugal force acting on it, and thus consistently contributes to the formation of a magnetodisc structure in a predictable way (e.g. ?).

In addition, due to the local and global variability in the hot plasma population, it is difficult to study its impact on magnetodisc structure based on *in situ* measurements alone, as a local measurement of plasma properties does not necessarily reveal information about the large-scale distribution of plasma throughout the magnetosphere. The UCL/AGA model is therefore particularly well suited to use as a tool to investigate this issue, as the hot plasma pressure throughout the magnetosphere can be simply parameterised in the model, in line with the expected range based on *in situ* observations, and the corresponding affect on the magnetodisc structure can be readily investigated.

In Chapters ?? and ??, we presented results which suggest that in general a globally enhanced hot plasma pressure causes a more disc-like magnetic field structure, with more radially stretched magnetic field lines in the middle magnetosphere. A similar result was found in ?, who compared two UCL/AGA models calculated with different hot plasma states. This reconfiguration is due to the enhancement of the equatorial ring current intensity associated with a greater hot plasma population, and the associated magnetic field causing a more significant distortion from a dipole in such conditions. This ring current intensity enhancement, and an associated enhancement in equatorial magnetic field strength, is demonstrated explicitly in Chapter ??, when comparing magnetic field profiles for UCL/AGA models representing different local time sectors, with different typical hot plasma pressure profiles.

It was shown by ? that in general the pressure associated with the hot plasma population was enhanced in the dusk and night local time sectors compared to noon and dawn, and that this suggested an asymmetry in the equatorial profiles of magnetic field strength; of particular interest perhaps was a small between dawn and dusk, with higher magnetic field strength in general at dusk which would be unlikely to reveal itself in noisy *in situ* magnetic field observations. This hot plasma pressure asymmetry also caused a more distorted magnetodisc structure with thinner current sheet at the dusk sector under some conditions; however due to the aforementioned dawn-dusk asymmetry also in system size, this effect was comparable and opposite to the more disc-like structure generated at dawn due to the increased system size there.

In terms of dynamics, in Chapter ?? we showed that the hot plasma population also influenced magnetospheric compressibility, increasing the sensitivity of the magnetosphere to changing solar wind conditions with comparable influence as a variation in system size. This is partially explained by the aforementioned reconfiguration of the magnetospheric magnetic field in such conditions, with associated magnetic field pressure varying more slowly with radial distance for systems with higher hot plasma content, and therefore being more easily compressible. However we also showed that, in our UCL/AGA model calculations, for a magnetosphere with sufficiently high hot plasma content still in line with observations from ?, the plasma β associated with the hot plasma population at the boundary surpassed 1. This means that, under such conditions, the behaviour of the hot plasma pressure, and how it varies with radial distance, becomes important in determining pressure balance at the magnetopause boundary, and thus controlling magnetospheric compressibility. We found that the hot plasma pressure typically varied even more slowly with radial distance than the magnetic pressure associated with a magnetodisc field structure, and thus the magnetosphere became more easily compressible under such conditions. A recent empirical study on the size and shape of Saturn's magnetopause boundary by ?, also found evidence that the magnetospheric compressibility behaviour was likely influenced by the magnetosphere's internal plasma state. However as they were limited to using single-point *in situ* observations of magnetospheric conditions, they could only investigate the relationship with the local plasma β mea-

sured at the magnetopause crossing location, rather than the global state of the hot plasma population in the magnetosphere.

3.3 Impact of Periodic Magnetic Perturbations on Large-Scale Structure and Dynamics

Cause a modulation of the thickness as well as the location. Variation on short timescales corresponding to beat period? Only way to explain Btheta.

3.4 Possible Directions for Future Work

3.4.1 Modifications to the UCL/AGA Magnetodisc Model

- make more parameters LT dependent - segment them into smaller LT sectors once more data is available to make it properly 3D - pressure anisotropy e.g. Nichols paper

3.4.2 Investigations into Periodic Magnetic Perturbations

- recent collaboration opportunities to continue working on equinox study using a combination of northern and southern periodicities - empirical studies of local time variation in current sheet thickness e.g. Ned

3.4.3 Looking Further Afield

- more large-scale, with the end of Cassini, more people moving to Jupiter. Juno may answer some questions, allow a comparison of the compressibility with more detail. JUICE. Exoplanet discoveries of magnetospheres.